Cell Stem Cell

Article

Dietary suppression of MHC class II expression in intestinal epithelial cells enhances intestinal tumorigenesis

Graphical abstract

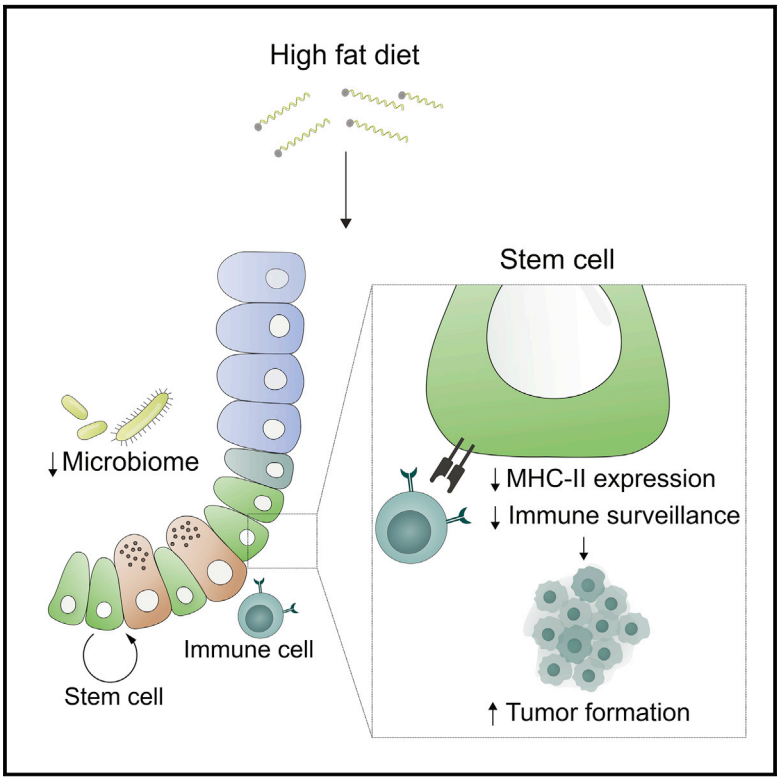

Highlights

- HFD dampens MHC class II expression in IECs, including ISCs
- HFD perturbs intestinal microbes that correlate with MHC class II expression in ISCs
- PRR and IFNγ signaling mediates epithelial MHC class II expression
- Loss of MHC class II on premalignant ISCs enhances tumor initiation

Authors

Semir Beyaz, Charlie Chung, Haiwei Mou, ..., Jatin Roper, Stuart H. Orkin, Ömer H. Yilmaz

Correspondence

beyaz@cshl.edu (S.B.), stuart_orkin@dfci.harvard.edu (S.H.O.), ohyilmaz@mit.edu (Ö.H.Y.)

In brief

The mechanisms that link pro-obesity high-fat diets (HFDs) to increased colon cancer risk are not well understood. Beyaz and colleagues demonstrate that a HFD promotes intestinal tumor initiation by suppressing microbiome-stem cell-immune cell crosstalk that is mediated by MHC class II expression on intestinal stem cells.

Beyaz et al., 2021, Cell Stem Cell *28*, 1–14
November 4, 2021
https://doi.org/10.1016/j.stem.2021.08.007

CellPress

Cell Stem Cell

CellPress

Article

Dietary suppression of MHC class II expression in intestinal epithelial cells enhances intestinal tumorigenesis

Semir Beyaz,[1,2,3,17,*] Charlie Chung,[1] Haiwei Mou,[1] Khristian E. Bauer-Rowe,[3] Michael E. Xifaras,[1,3] Ilgin Ergin,[1] Lenka Dohnalova,[4] Moshe Biton,[5,6] Karthik Shekhar,[5,7] Onur Eskiocak,[1] Katherine Papciak,[1] Kadir Ozler,[1] Mohammad Almeqdadi,[3] Brian Yueh,[1] Miriam Fein,[1] Damodaran Annamalai,[8] Eider Valle-Encinas,[3] Aysegul Erdemir,[3] Karoline Dogum,[3] Vyom Shah,[1] Aybuke Alici-Garipcan,[1] Hannah V. Meyer,[1] Deniz M. Özata,[9] Eran Elinav,[10] Alper Kucukural,[11] Pawan Kumar,[12] Jeremy P. McAleer,[13] James G. Fox,[8] Christoph A. Thaiss,[4] Aviv Regev,[3,5,14] Jatin Roper,[15] Stuart H. Orkin,[2,*] and Ömer H. Yilmaz[3,16,*]

[1]Cold Spring Harbor Laboratory, Cold Spring Harbor, NY 11724, USA
[2]Division of Hematology/Oncology, Boston Children's Hospital and Department of Pediatric Oncology, Dana-Farber Cancer Institute, Howard Hughes Medical Institute, Harvard Stem Cell Institute, Harvard Medical School, Boston, MA 02115, USA
[3]The David H. Koch Institute for Integrative Cancer Research at MIT, Department of Biology, MIT, Cambridge, MA 02139, USA
[4]Department of Microbiology, Perelman School of Medicine, University of Pennsylvania, Philadelphia, PA 19104, USA
[5]Klarman Cell Observatory, Broad Institute of Harvard and MIT, Cambridge, MA 02142, USA
[6]The Department of Biological Regulation, Weizmann Institute of Science, Rehovot 7610001, Israel
[7]Department of Chemical and Biomolecular Engineering, Helen Wills Neuroscience Institute, University of California, Berkeley, CA 94720, USA
[8]Division of Comparative Medicine, Department of Biological Engineering, Massachusetts Institute of Technology, Cambridge, MA 02139, USA
[9]RNA Therapeutics Institute, University of Massachusetts Medical School, Worcester, MA 01605, USA
[10]Department of Immunology, Weizmann Institute of Science, Rehovot 7610001, Israel
[11]Program in Molecular Medicine, University of Massachusetts Medical School, Worcester, MA 01605, USA
[12]Department of Microbiology and Immunology, Renaissance School of Medicine, Stony Brook University, Stony Brook, NY 11794, USA
[13]Department of Pharmaceutical Science and Research, Marshall University School of Pharmacy, Huntington, WV 25701, USA
[14]Howard Hughes Medical Institute, Department of Biology, Massachusetts Institute of Technology, Cambridge, MA 02140, USA
[15]Department of Medicine, Division of Gastroenterology, Duke University, Durham, NC 27710, USA
[16]Department of Pathology, Massachusetts General Hospital and Harvard Medical School, Boston, MA 02114, USA
[17]Lead contact
*Correspondence: beyaz@cshl.edu (S.B.), stuart_orkin@dfci.harvard.edu (S.H.O.), ohyilmaz@mit.edu (Ö.H.Y.)
https://doi.org/10.1016/j.stem.2021.08.007

SUMMARY

Little is known about how interactions of diet, intestinal stem cells (ISCs), and immune cells affect early-stage intestinal tumorigenesis. We show that a high-fat diet (HFD) reduces the expression of the major histocompatibility complex class II (MHC class II) genes in intestinal epithelial cells, including ISCs. This decline in epithelial MHC class II expression in a HFD correlates with reduced intestinal microbiome diversity. Microbial community transfer experiments suggest that epithelial MHC class II expression is regulated by intestinal flora. Mechanistically, pattern recognition receptor (PRR) and interferon-gamma (IFNγ) signaling regulates epithelial MHC class II expression. MHC class II-negative (MHC-II−) ISCs exhibit greater tumor-initiating capacity than their MHC class II-positive (MHC-II+) counterparts upon loss of the tumor suppressor Apc coupled with a HFD, suggesting a role for epithelial MHC class II-mediated immune surveillance in suppressing tumorigenesis. ISC-specific genetic ablation of MHC class II increases tumor burden cell autonomously. Thus, HFD perturbs a microbiome-stem cell-immune cell interaction that contributes to tumor initiation in the intestine.

INTRODUCTION

Diet is a major lifestyle factor that influences health and disease states, including cancer (Beyaz and Yilmaz, 2016; Zitvogel et al., 2017). Significant epidemiologic and preclinical studies link long-term dietary patterns such as western diets and obesity to several types of cancer, including colorectal cancer. However, how the adaptation of the intestinal epithelium to pro-obesity diets alters cancer risk remains elusive (Basen-Engquist and Chang, 2011; Calle et al., 2003; Gallagher and LeRoith, 2015). The intestinal epithelium is maintained by Lgr5+ intestinal stem cells (ISCs) that reside at the crypt base and give rise to the

Please cite this article in press as: Beyaz et al., Dietary suppression of MHC class II expression in intestinal epithelial cells enhances intestinal tumorigenesis, Cell Stem Cell (2021), https://doi.org/10.1016/j.stem.2021.08.007

diverse, specialized cell types of the intestinal lining (Barker et al., 2007). These rapidly renewing ISCs coordinate intestinal adaptation in response to environmental inputs such as diet by balancing stem cell self-renewal with differentiation divisions (Beyaz et al., 2016; Wang et al., 2018; Yang et al., 2008; Yilmaz et al., 2012). ISCs are also the cells of origin for many early intestinal tumors and lie at the interface of dietary nutrients, commensal microbes, and immune cells. Thus, understanding how diet induces changes in ISCs and their surrounding components may shed light on the early steps involved in initiation of colorectal cancers (Barker et al., 2009; Belkaid and Hand, 2014; Clevers, 2013; Hooper et al., 2012; Thaiss et al., 2016).

Diet contributes to colorectal cancer risk through diverse cancer-cell-intrinsic and cancer-cell-extrinsic mechanisms. Although accumulating evidence demonstrates that pro-obesity or western diets enhance intestinal tumorigenesis in many ways, such as through activation of lipid-sensing PPAR transcription factors (Beyaz et al., 2016, 2021), bile acids (Fu et al., 2019a), alteration of vitamin D signaling (Li et al., 2019), inflammation (Font-Burgada et al., 2016), and the microbiome (Schulz et al., 2014), the role that immune cells play in this process is unclear. Because interactions between the cancer cells and the immune system influence tumor initiation and progression, it is important to understand the crosstalk between tumor-initiating ISCs and immune cells. Recognition of antigens by T cells through antigen presentation pathways is a major mechanism for triggering anti-tumor immunity (Sade-Feldman et al., 2017; Vanneman and Dranoff, 2012). Although major histocompatibility complex class I (MHC class I) antigen presentation pathway-mediated activation of cytotoxic CD8+ T cells plays a major role in anti-tumor immune responses, MHC class II-mediated activation of CD4+ T cells is also pivotal for tumor immunity. CD4+ T cells can help in the maintenance of CD8+ T cell responses and produce cytokines that shape the overall response against the tumor (Haabeth et al., 2016; Hirschhorn-Cymerman et al., 2012; Hung et al., 1998; Tran et al., 2014; Xie et al., 2010; Zhang et al., 2009). Although cancers develop several strategies to evade the immune system (Grasso et al., 2018; Liu et al., 2017), little is known about how diet-induced obesity affects the immune recognition of ISCs during tumor initiation.

RESULTS

HFD dampens epithelial MHC class II expression

To explore how a high-fat diet (HFD) perturbs immunomodulatory gene expression in ISCs, we examined our previous mRNA sequencing (mRNA-seq) dataset of Lgr5+ ISCs isolated from control and HFD-fed mice (Beyaz et al., 2016). We found that Lgr5+ ISCs derived from HFD-fed mice significantly downregulate immunomodulatory genes that are involved in the MHC class II pathway (*H2-Aa*, *H2-Ab1*, and *Ciita*), anti-microbial response/inflammation (*Reg3g* and *Nfkb2*), and costimulation (*Icosl*, *Sectm1a*, and *Sectm1b*) (Choi et al., 2011; Dong et al., 2001; Howie et al., 2013; Mukherjee and Hooper, 2015; Tomas et al., 2016) (Figures 1A and S1A). Given the recently reported heterogeneity within Lgr5+ ISCs (Barriga et al., 2017; Biton et al., 2018), we next performed single-cell RNA sequencing (scRNA-seq) of Lgr5+ ISCs derived from control or HFD mice. Consistent with the bulk RNA sequencing (RNA-seq) profiles, *H2-Ab1*, a key component of the MHC class II complex, was among the top 5 differentially expressed genes, with >3-fold higher expression in control compared with HFD ISCs (Figures 1B, S1B, and S1C; see STAR Methods) (Model-based Analysis of Single-cell Transcriptomics [MAST] test, $p < 1e{-}10$). To determine the extent of MHC class II downregulation in response to HFD in our scRNA-seq data, we ranked individual ISCs based on their expression pattern of MHC class II pathway genes (MHC class II score) (Table S1) and found that HFD Lgr5+ ISCs had a consistently lower MHC class II score compared with control Lgr5+ ISCs (Figure 1C). We then selected the upper and lower quartiles in scRNA-seq data and performed differential expression analysis between MHC class II-low and MHC class II-high HFD Lgr5+ ISCs. As expected, MHC class II pathway genes (*H2-Ab1*, *Cd74*, *H2-Aa*, and *H2-DMa*) were among the top upregulated genes in MHC class II-high cells (Figure 1D).

Although MHC class II expression and function are generally considered restricted to professional antigen-presenting cells, several studies have demonstrated that intestinal epithelial cells (IECs) express high levels of MHC class II and are able to capture, process, and present antigens to CD4+ T cells; this includes work from our group on ISCs (Biton et al., 2018; Cerf-Bensussan et al., 1984; Dahan et al., 2007; Hershberg et al., 1997; Telega et al., 2000; Thelemann et al., 2014; Westendorf et al., 2009) (Figure S1G). We validated the reduction of MHC II expression on IECs and Lgr5+ ISCs under a HFD in several ways. *In situ* hybridization for *H2-Ab1* showed that MHC class II is expressed in the epithelium of control mice but has diminished expression throughout the epithelium of HFD mice, including in the intestinal crypt where ISCs reside (Figure 1E). Moreover, by flow cytometry, both Epcam+ IECs (Figures 1F and 1G) and Lgr5+ ISCs (Figures 1I and 1J) expressed high levels of MHC class II protein on their cell surface at steady state, and this expression was significantly downregulated in response to a HFD. Finally, we confirmed that sorted Epcam+ IECs (Figure 1H) and Lgr5+ ISCs (Figure 1K) from HFD-fed mice significantly downregulated MHC class II expression by qPCR. We then partitioned Lgr5+ ISCs into two subpopulations based on their MHC class II expression pattern, MHC class II-positive (MHC-II+) and MHC class II-negative (MHC-II−), and assessed their frequencies in control or HFD-fed mice. Although in control mice most Lgr5+ ISCs were MHC-II+, a HFD led to a significant reduction in the frequency of MHC-II+ Lgr5+ ISCs and to a concomitant increase in the frequency of MHC-II− Lgr5+ ISCs (Figures 1L and 1M). We sorted these ISC subpopulations to confirm MHC class II expression levels. Consistent with our scRNA-seq analysis, the expression levels of *H2-Ab1* mRNA were significantly reduced in response to HFD (Figure S1D). Altogether, these results indicate that HFD leads to suppression of MHC class II expression in Epcam+ IECs, including Lgr5+ ISCs.

PPAR-δ activation or obesity does not affect MHC class II expression in Lgr5+ ISCs

A HFD perturbs multiple epithelial-intrinsic and epithelial-extrinsic pathways that may influence the regulation of MHC class II expression in ISCs (Fu et al., 2019a; Schulz et al., 2014). Because our prior findings demonstrated that a PPAR-δ program mediates many effects of a HFD in Lgr5+ ISCs (Beyaz et al., 2016, 2021), we next assessed the activation status of a

Please cite this article in press as: Beyaz et al., Dietary suppression of MHC class II expression in intestinal epithelial cells enhances intestinal tumorigenesis, Cell Stem Cell (2021), https://doi.org/10.1016/j.stem.2021.08.007

CellPress

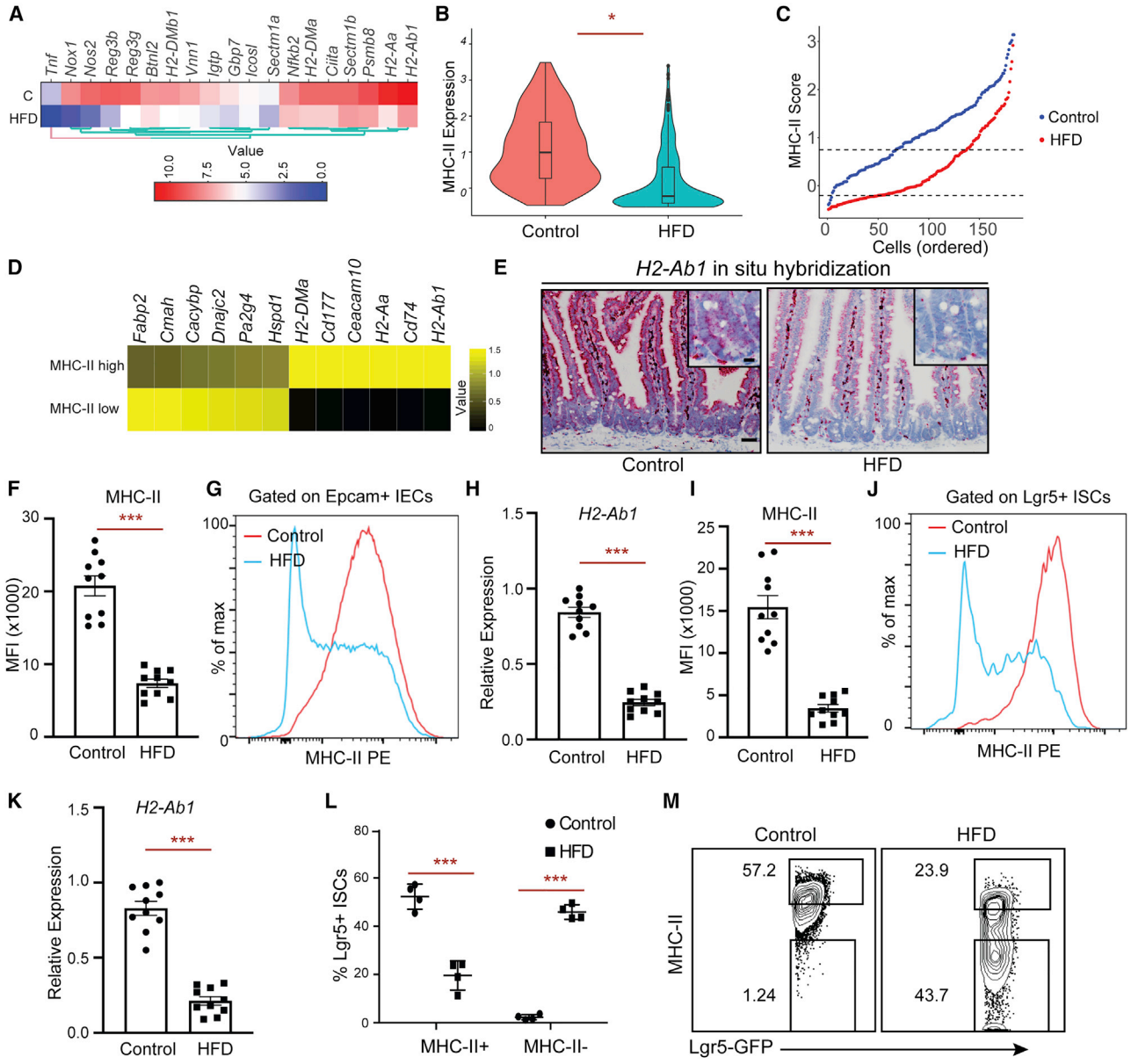

Figure 1. High-fat diet reduces MHC class II expression on Lgr5-GFP^{hi} (Lgr5+) intestinal stem cells (ISCs)

(A) Heatmap of downregulated genes assessed by bulk RNA-seq in Lgr5+ ISCs isolated from long-term high-fat-diet (HFD)-fed mice compared with control mice (n = 2). The scale represents computed *Z* scores of log10 expression values.

(B) Violin plots demonstrating MHC class II expression in single Lgr5+ ISCs isolated from control (n = 171 cells, 2 independent experiments) or HFD mice by single-cell RNA-seq (scRNA-seq) (n = 144 cells, 2 independent experiments) (MAST test, $p < 1e{-}10$).

(C) Control (blue) and HFD (red) Lgr5+ ISCs ranked according to their expression of MHC II pathway genes (y axis). Dashed lines correspond to y intercepts of −0.2 and 0.75, which are the 25th and 75th percentile of scores in HFD cells, used to define MHC class II-low (score < −0.2) and MHC class II-high (score > 0.75) HFD cells. In contrast, these values correspond to 1st and 35th percentile of scores in control cells.

(D) Heatmap showing differentially expressed (DE) genes (rows) between MHC class II-low and MHC class II-high HFD ISCs as defined in (C). The scale represents computed *Z* scores of log10 expression values.

(E) Single-molecule *in situ* hybridization of MHC class II (*H2-Ab1*) in control and HFD mice (n = 5). Scale bars, 50 μm (E) and 20 μm (E, inset).

(F and G) Mean fluorescence intensity (MFI) of MHC class II in Epcam+ intestinal epithelial cells (IECs) from crypts of control and HFD mice (F) (n = 10 mice, mean ± SEM). Representative flow cytometry histogram plots of MHC class II expression in Epcam+ IECs (G).

(H) Relative expression of MHC class II (*H2-Ab1*) in Epcam+ IECs isolated from crypts of control and HFD mice (n = 10 mice, mean ± SEM).

(I and J) MFI of MHC class II in Lgr5+ ISCs from crypts of control and HFD mice (I) (n = 10 mice, mean ± SEM). Representative flow cytometry histogram plots of MHC class II expression in Epcam+ cells (J).

(K) Relative expression of MHC class II (*H2-Ab1*) in Lgr5+ ISCs isolated from crypts of control and HFD mice (n = 10 mice, mean ± SEM).

(L and M) Frequency of MHC-II+ and MHC-II− Lgr5+ ISCs in control and HFD mice by flow cytometry (L) (n = 4, mean ± SD). Representative flow cytometry plots of MHC class II in control and HFD ISCs (M).

*p < 0.05, **p < 0.01, ***p < 0.001 (Student's t tests). Scale bars, 50 μm (E) and 20 μm (E, inset). See also Figure S1 and Table S1.

Please cite this article in press as: Beyaz et al., Dietary suppression of MHC class II expression in intestinal epithelial cells enhances intestinal tumorigenesis, Cell Stem Cell (2021), https://doi.org/10.1016/j.stem.2021.08.007

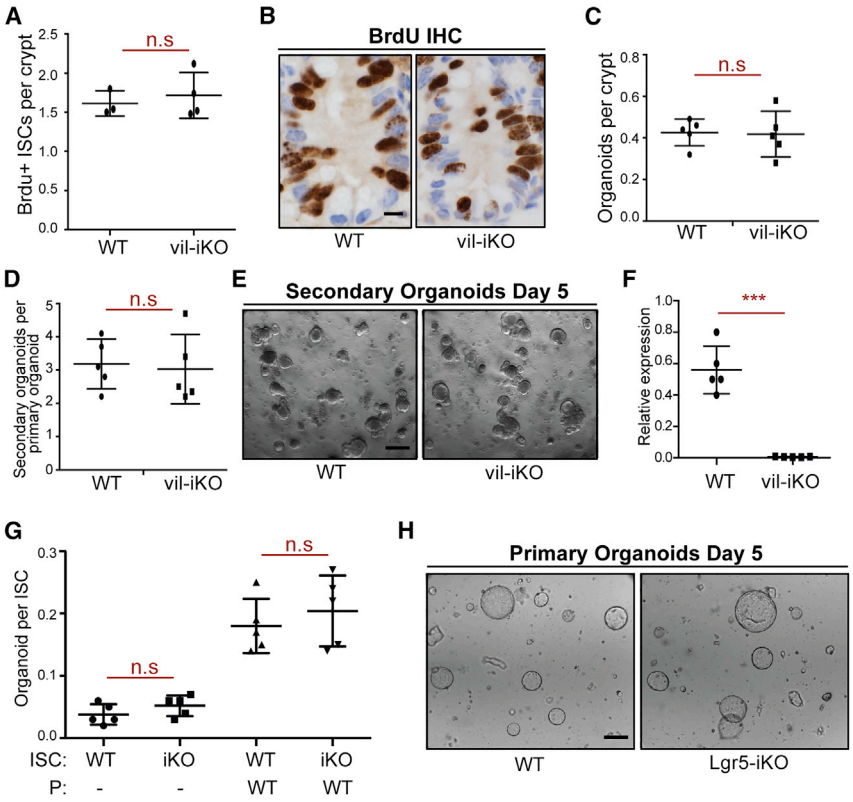

Figure 2. Intestine-specific deletion of MHC class II does not alter the organoid-forming capacity of ISCs

(A and B) Number of bromodeoxyuridine (BrdU)+ crypt base columnar cells after a 4-h pulse in Villin-CreERT2; MHC-II$^{L/L}$ (vil-iKO) mice after tamoxifen administration (WT, n = 3; vil-iKO, n = 4; mean ± SD). Representative images of BrdU immunostain in proximal small intestinal crypts (B).

(C–E) Organoid-initiating capacity of WT and vil-iKO crypts (C) (n = 5, mean ± SD). Number of secondary organoids per dissociated crypt-derived primary organoid (D) (n = 5, mean ± SD). Representative images of day-5 WT and vil-iKO primary organoids (E).

(F) Relative expression of MHC class II in dissociated WT and vil-iKO primary organoids at day 5 (n = 5, mean ± SD).

(G and H) Organoid-initiating capacity of ISCs from WT and Lgr5-EGFP-IRES-CreERT2; MHC-II$^{L/L}$ (Lgr5-iKO) mice with and without Paneth cells (P) from WT mice (n = 5, mean ± SD). Representative images of organoids derived from WT and Lgr5-iKO ISCs cocultured with WT Paneth cells five days after seeding (H).

n.s., not significant; ***p < 0.001 (Student's t tests). Scale bars, 100 μm (E and H) and 20 μm (B). See also Figure S2.

PPAR-δ program in Lgr5+ ISCs based on their MHC class II expression pattern in response to a HFD. We found no difference in the expression levels of PPAR-δ-induced signature genes *Hmgcs2* and *Jag1* or the stem cell marker *Lgr5* in MHC-II+ and MHC-II− ISCs in either cohort (Figure S1E). Interestingly, agonist-induced PPAR-δ activation with GW501516 also did not reduce MHC class II expression in Lgr5+ ISCs, indicating that HFD-induced MHC class II downregulation is independent of PPAR-δ activity in ISCs (Figures S1I and S1J). To determine whether MHC class II expression in Lgr5+ ISCs is reduced in an independent model of obesity, we examined leptin-receptor-deficient (db/db) mice, an obesity model that develops on a control diet (Coleman, 1978). (Figure S1H). Lgr5+ ISCs isolated from both lean control (db/+) and obese (db/db) mice expressed high levels of MHC class II, indicating that diet-induced alterations, rather than obesity per se, inhibit MHC class II expression in ISCs (Figures S1K and S1L).

Epithelial MHC class II expression does not influence organoid-forming capacity of ISCs

We next assessed whether HFD-mediated downregulation of MHC class II affects stemness. First, we assayed the functional potential of MHC-II+ and MHC-II− ISCs, using an *in vitro* approach based on the ability of isolated Lgr5+ ISCs to form organoid bodies in 3D culture (Beyaz et al., 2016; Sato et al., 2009). We found that MHC class II expression levels in control and HFD Lgr5+ ISCs did not affect *in vitro* organoid formation (Figure S1F). To further ascertain whether MHC class II expression regulates ISC function, we generated mice with intestinal epithelium-specific MHC class II deletion (vil-iKO; see STAR Methods). Intestine-specific loss of MHC class II did not affect the weight and length of the small intestine or affect crypt depth and villi height (Figures S2A–S2G). Furthermore, the proliferation or organoid-forming capacity of ISCs was unaltered upon loss of MHC class II in the intestinal epithelium (Figures 2A–2F). To assess how MHC class II regulates ISC function specifically, we ablated MHC class II in Lgr5+ ISCs (Lgr5-iKO; Figure S2H; see STAR Methods) and found that loss of MHC class II in Lgr5+ ISCs and their progenies did not affect the capacity of ISCs to initiate organoids (Figures 2G and 2H). To determine how MHC class II influences Lgr5+ ISC function *in vivo*, we performed LacZ lineage-tracing analysis and did not detect differences in the generation of LacZ+ cells between wild-type (WT) and Lgr5-iKO mice (Figure S2I). Although these data illustrate that the *in vitro* organoid-forming capacity of Lgr5+ ISCs is independent of MHC class II expression and that MHC class II loss does not alter intestinal homeostasis and ISC output (i.e., LacZ+ progeny) at steady state, MHC class II likely influences ISC differentiation by engaging T helper cell cytokines in the context of inflammation, as we have previously reported (Biton et al., 2018).

Epithelial MHC class II expression depends on the intestinal microbiome

The intestinal microbiome plays a significant role in regulating intestinal immunity (Belkaid and Hand, 2014; David et al., 2014; Hooper et al., 2012; Round and Mazmanian, 2009; Thaiss et al., 2016). Because dietary perturbations are among the major external factors shaping the intestinal microbiome, we asked whether HFD-induced alterations in the microbiome influence MHC class II expression in IECs and ISCs. To determine whether

Please cite this article in press as: Beyaz et al., Dietary suppression of MHC class II expression in intestinal epithelial cells enhances intestinal tumorigenesis, Cell Stem Cell (2021), https://doi.org/10.1016/j.stem.2021.08.007

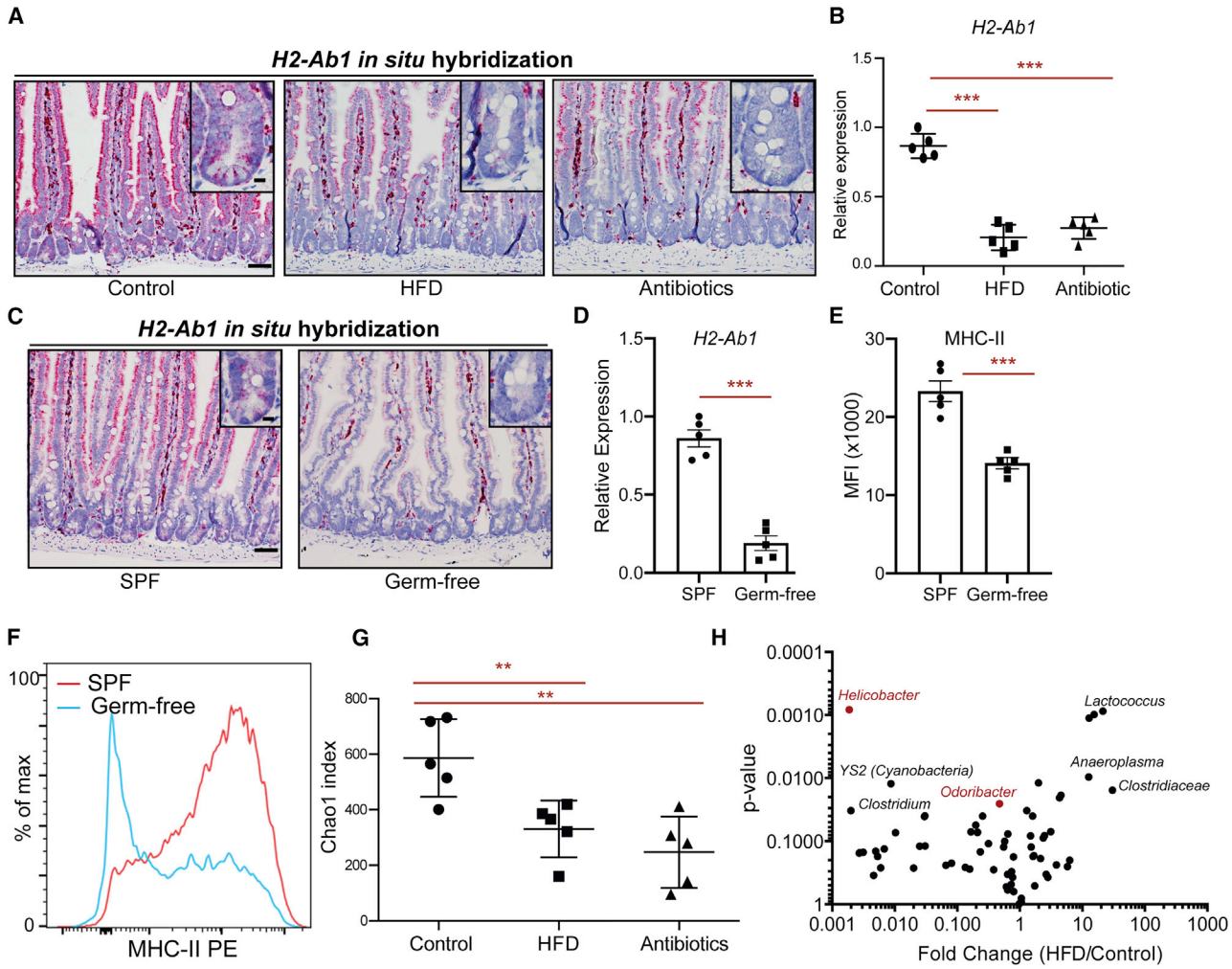

Figure 3. Intestinal microbiome regulates epithelial MHC class II expression

(A) *In situ* hybridization for *H2-Ab1* in control, HFD, and antibiotic-treated mice in the proximal small intestine (n = 5 mice).

(B) Relative expression of MHC class II in Lgr5+ ISCs from control, HFD, and antibiotic-treated mice (n = 5, mean ± SD).

(C) Single-molecule *in situ* hybridization of MHC class II (*H2-Ab1*) in specific pathogen-free (SPF) and germ-free mice (n = 5 mice).

(D) Relative expression of MHC class II (*H2-Ab1*) in Lgr5+ ISCs from SPF and germ-free mice (n = 5, mean ± SEM).

(E and F) MFI of MHC class II in Lgr5+ ISCs from SPF and germ-free mice (E) (n = 5, mean ± SEM). Representative flow cytometry histogram plots of MHC class II expression in Lgr5+ ISCs (F).

(G) Chao1 index of microbial diversity in control, HFD, and mice treated with antibiotics for 3 months (n = 5, mean ± SD).

(H) Volcano plot demonstrating significantly enriched and depleted microbial species in HFD versus control mice (n = 5).

**p < 0.01, ***p < 0.001 (Student's t tests). Scale bars, 100 μm (A and C) and 20 μm (A and C, insets). See also Figure S2.

the microbiome is involved in regulation of epithelial MHC class II levels, we treated mice with broad-spectrum antibiotics, which ablated bacterial diversity and massively altered community composition (Figure S2J). Similar to a HFD, antibiotic treatment was accompanied by decreased MHC class II expression in Lgr5+ ISCs and the intestinal epithelium (Figures 3A and 3B) comparable with that observed in HFD. To corroborate the role of the intestinal microbiome on MHC class II expression on ISCs, we generated germ-free Lgr5-GFP-IRES-CreERT2 mice. Lgr5+ ISCs from germ-free mice exhibited reduced MHC class II expression at both RNA and protein levels compared with specific pathogen-free control mice (Figures 3C–3F, S2J, and S2K).

Helicobacter colonization correlates with epithelial MHC class II expression

To gain insight into the spectrum of members of the bacterial microbiome capable of inducing epithelial MHC class II expression, we performed comparative 16S rDNA sequencing in fecal DNA isolated from HFD-treated mice and controls. Consistent with previous reports, HFD-induced obesity led to microbial dysbiosis with reduced bacterial diversity in the feces (Figures 3G and S2J) (Ley et al., 2005; Schulz et al., 2014). Among the bacterial genera strongly diminished under HFD conditions was *Helicobacter* (Figure 3H). To determine whether *Helicobacter* colonization in mice correlates with epithelial MHC class II expression in the intestine, we surveyed our mouse facility for presence or

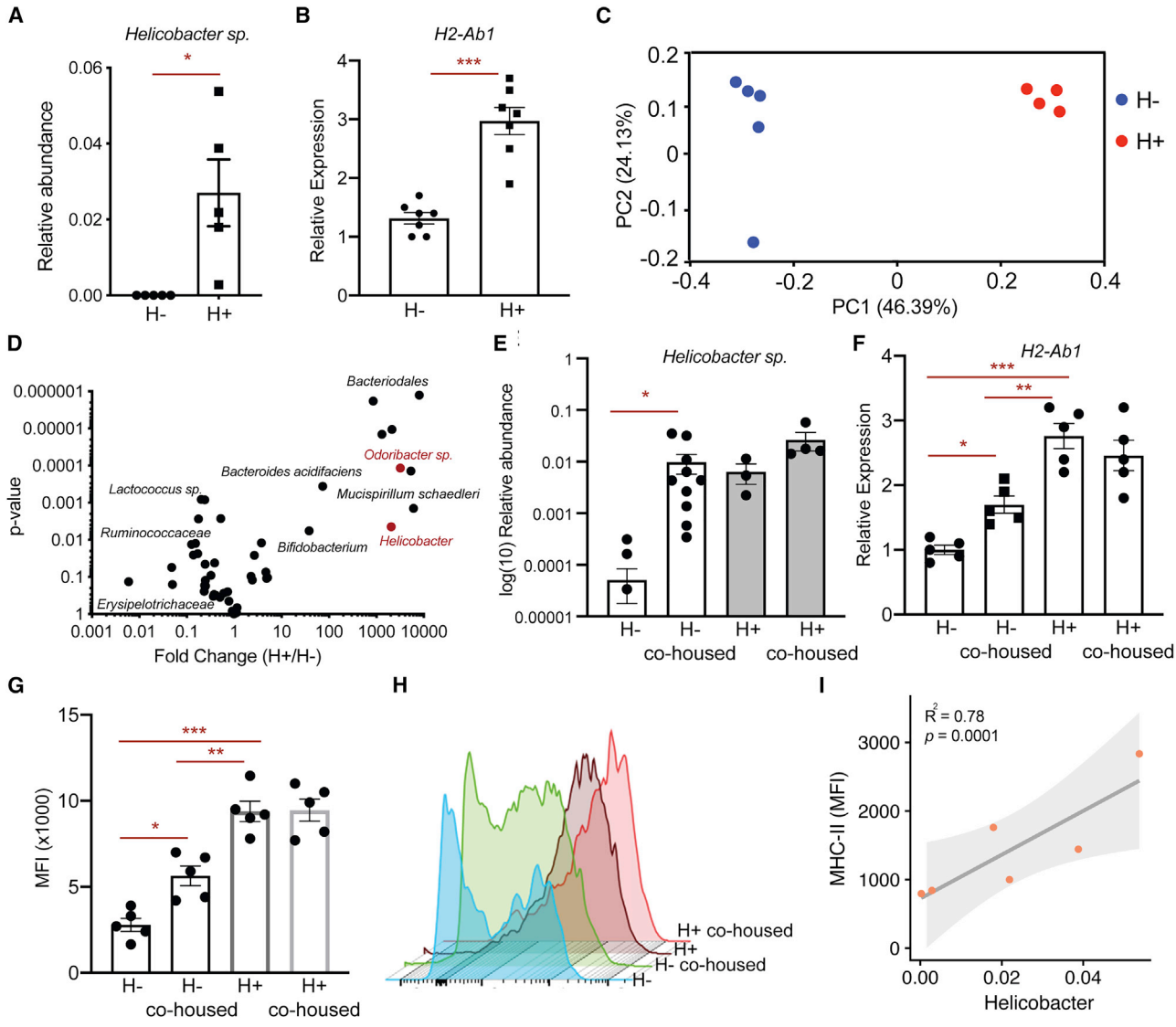

Figure 4. *Helicobacter* colonization correlates with epithelial MHC class II expression

(A) Relative abundance of *Helicobacter* spp. in mice housed in a clean (H^-) room and a dirty (H^+) room (n = 5 mice, mean ± SEM).

(B) Relative expression of MHC class II (*H2-Ab1*) in Epcam+ cells isolated from crypts of mice housed in the H^- room or H^+ room (n = 7, mean ± SEM).

(C) Principal coordinate analysis (PCoA) of the microbial composition in feces of mice housed in the H^- room or H^+ room (n = 5).

(D) Volcano plot demonstrating significantly enriched and depleted microbial species in mice housed in the H^+ room versus the H^- room (n = 5).

(E) Relative abundance of *Helicobacter* sp. in mice housed in either the H^- room (n = 10) or the H^+ room (n = 3) or after cohousing H^- mice (n = 10) with H^+ mice (n = 4) in the H^+ room (mean ± SEM).

(F) Relative expression of MHC class II (*H2-Ab1*) in Epcam+ cells isolated from crypts of mice housed in either the H^- room or the H^+ room or after cohousing H^- mice with H^+ mice in the H^+ room (n = 5, ANOVA).

(G and H) MFI of MHC class II in Epcam+ cells isolated from crypts of mice housed in either the H^- room or the H^+ room or after cohousing H^- mice with H^+ mice in the H^+ room (G) (n = 5, mean ± SEM, ANOVA). Representative flow cytometry histogram plots of MHC class II expression in Lgr5+ ISCs (H).

(I) Correlation of MHC class II expression with *Helicobacter* abundance in germ-free mice that were transplanted with fecal content from H^- and H^+ mice.

Unless otherwise indicated *p < 0.05, **p < 0.01, ***p < 0.001 (Student's t tests). See also Figure S2 and Table S2.

absence of *Helicobacter* species in mice housed in different rooms. We created two separate rooms with mice either naturally colonized with *Helicobacter* species (H^+, dirty room) or without detectable *Helicobacter* species (H^-, clean room) (Figure 4A). *Helicobacter* species that naturally colonize mice in the H^+ room and are absent from the H^- room include *Helicobacter mastomyrinus* and *Helicobacter typhlonius* (Table S2). Interestingly, MHC class II expression was significantly higher in the intestinal epithelium of mice that are housed in the H^+ room compared with the mice housed in the H^- room (Figure 4B). Comparison of microbial composition between H^+ mice and H^- mice revealed bacteria that are more abundant in H^+ mice and associate with high epithelial MHC class II expression (Figures 4C and 4D). These include *Helicobacter* sp. (Figures 4A and

Please cite this article in press as: Beyaz et al., Dietary suppression of MHC class II expression in intestinal epithelial cells enhances intestinal tumorigenesis, Cell Stem Cell (2021), https://doi.org/10.1016/j.stem.2021.08.007

CellPress

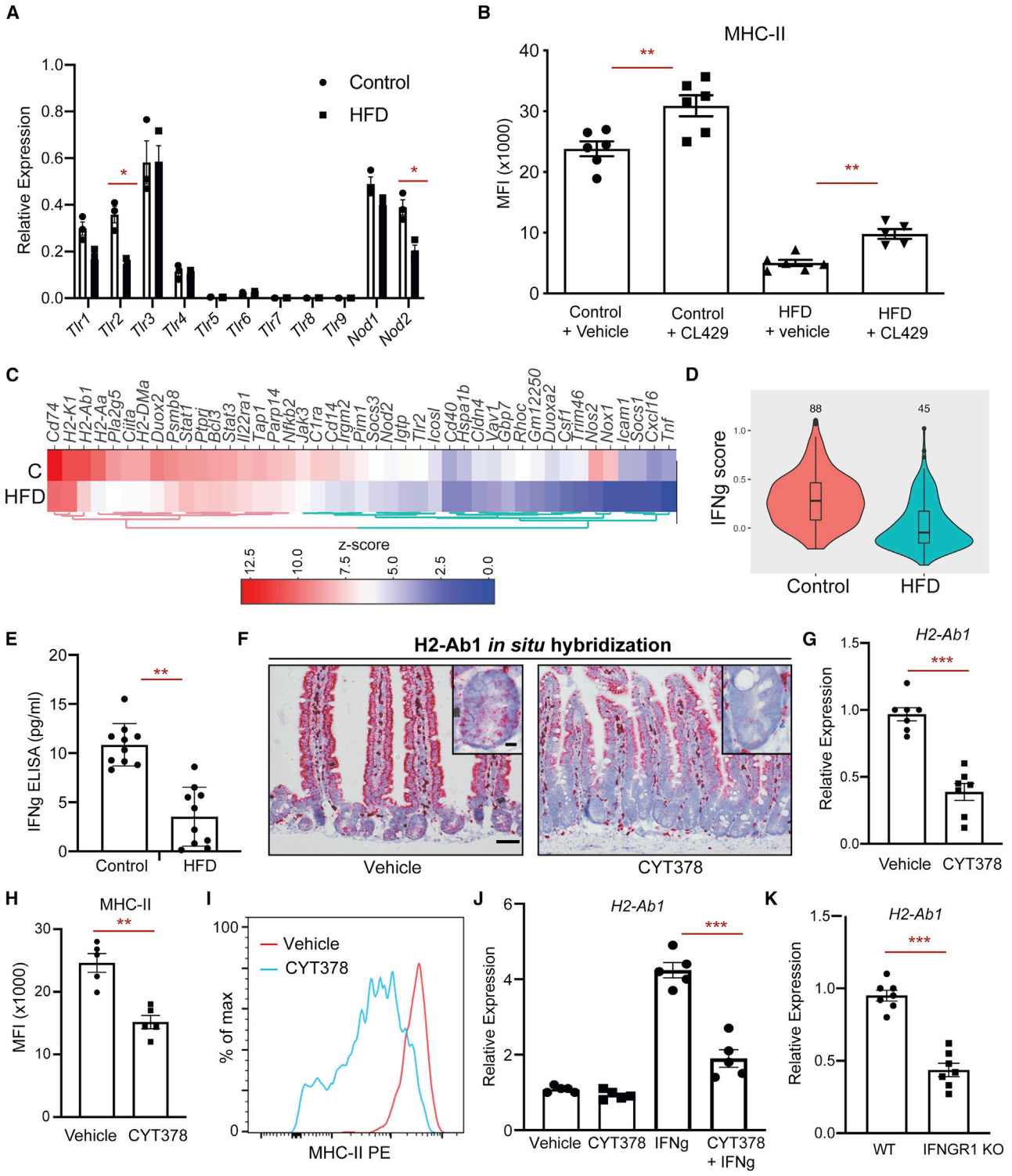

Figure 5. PRR and IFNγ signaling regulates epithelial MHC class II expression

(A) Relative expression of pattern recognition receptors (PRRs) in control and HFD ISCs (n = 3).

(B) MFI of MHC class II in Lgr5+ ISCs from vehicle- and TLR2/NOD2 agonist CL429-treated control and HFD mice (n = 6 mice, mean ± SEM).

(C) Heatmap of expression levels of IFNγ-induced genes between HFD and control Lgr5+ ISCs by bulk RNA-seq (n = 2). The scale represents computed *Z* scores of log10 expression values.

(D) Violin plots demonstrating the expression levels of IFNγ-induced genes in control and HFD Lgr5+ ISCs by scRNA-seq.

(E) IFNγ levels in the intestines of control and HFD mice as measured by ELISA (n = 10, mean ± SEM).

(legend continued on next page)

Please cite this article in press as: Beyaz et al., Dietary suppression of MHC class II expression in intestinal epithelial cells enhances intestinal tumorigenesis, Cell Stem Cell (2021), https://doi.org/10.1016/j.stem.2021.08.007

4D) and *Odoribacter* sp. (Figures 4D and S2L), which were both reduced in response to HFD (Figure 3H). To determine whether colonization of H^- mice with the microbial flora of H^+ mice enhances expression of epithelial MHC class II, we cohoused H^- mice with H^+ mice in the H^+ room (Figure S2M). Although H^- and H^+ mice have distinct microbial composition at baseline, as determined by principal coordinate analysis (PCoA), after cohousing the microbial profile of H^- mice resembles the H^+ mice (Figure S2M). Importantly, cohousing with H^+ mice led to a significant increase in both *Helicobacter* sp. and *Odoribacter* sp. abundance in the cohoused H^- mice, with a concomitant upregulation of epithelial MHC class II, compared with mice that remained in the H^- room (Figures 4E–4H and S2N). Finally, we performed fecal transplantation into gnotobiotic mice and found that *Helicobacter* colonization correlates with epithelial MHC class II expression levels in the intestine (Figure 4I). These results indicate that epithelial MHC class II expression is regulated by intestinal commensal bacteria, including *Helicobacter* sp., and is dampened in response to a HFD.

PRR and IFNγ signaling regulates epithelial MHC class II expression

Microbiome-induced activation of pattern recognition receptor (PRR) signaling or proinflammatory cytokines induces MHC class II expression in antigen-presenting cells and control intestinal homeostasis (Abreu, 2010; Rakoff-Nahoum et al., 2004; van den Elsen, 2011). To determine the necessity of PRR signaling through the adaptor protein Myd88 in regulating MHC class II expression, we generated intestine-specific Myd88-deficient mice (Myd88 iKO) and found significant downregulation of epithelial MHC class II compared with wild-type controls (Figures S3C and S3D). Next, we surveyed PRR expression patterns in ISCs in control and HFD conditions. Consistent with previous reports (Brown et al., 2014; Caruso et al., 2014; Neal et al., 2012; Price et al., 2018), ISCs expressed several Toll-like receptors (*Tlr1*, *Tlr2*, *Tlr3*, and *Tlr4*), as well as Nod-like receptors (*Nod1* and *Nod2*) (Figure 5A). Among these PRRs, *Tlr2* and *Nod2* were downregulated in response to a HFD (Figure 5A). To test whether activation of TLR2 and NOD2 pathways is sufficient to increase MHC class II expression in Lgr5+ ISCs, we treated mice with a dual TLR2/NOD2 agonist (CL429) (Pavot et al., 2014). Indeed, CL429 treatment led to significant upregulation of MHC class II in both control and HFD ISCs (Figures 5B, S3A, and S3B). Lastly, signaling through TLR2 and NOD2 induced MHC class II expression; however, it did not fully restore MHC class II levels of HFD-treated mice to control levels, suggesting that additional signaling pathways are needed to achieve baseline expression (Figures 5B, S3A, and S3B).

The intestinal microbiome also influences the activity of proinflammatory cytokine signaling, such as the proinflammatory cytokine interferon-gamma (IFNγ) and downstream JAK1/2 signaling pathways (van den Elsen, 2011). IFNγ is a potent inducer of MHC class II expression in antigen-presenting cells and other cell types, including intestinal epithelial cells (Collins et al., 1984; Thelemann et al., 2014; Wong et al., 1984). We examined the IFNγ responsiveness of MHC-II+ and MHC-II− HFD ISCs, which express similar levels of IFNγ receptor-1 (*Ifngr1*) and IFNγ receptor-2 (*Ifngr2*) (Figure S1E). IFNγ treatment led to upregulation of MHC class II in both MHC-II+ and MHC-II− Lgr5+ ISCs (Figure S3E). Although HFD Lgr5+ ISCs express lower levels of MHC class II, they are still responsive to IFNγ stimulation (Choi et al., 2011; Thelemann et al., 2014). To determine whether HFD leads to suppression of epithelial MHC class II expression by dampening IFNγ signaling, we assessed the expression levels of IFNγ-induced genes in control and HFD Lgr5+ ISCs. In response to HFD, we found that ISCs significantly downregulate IFNγ-induced genes, including MHC class II pathway genes (*H2-Ab1*, *H2-Aa*, *Ciita*, *Cd74*, and *H2-DMa*) and upstream pathway genes that regulate MHC class II expression (*Stat1*, *Stat3*, *Nfkb2*, and *Jak3*) (Figures 5C, 5D, S3F, and S3G). The levels of IFNγ were significantly reduced in the intestines of HFD mice compared with control mice (Figure 5E). Administration of a potent JAK1/2 and TBK1/IKKε inhibitor (CYT387) that inhibits both STAT and nuclear factor κB (NF-κB) signaling to mice significantly decreased MHC class II expression in Lgr5+ ISCs compared with vehicle-treated controls (Figures 5F–5I, S3H, and S3I) (Tyner et al., 2010). We next asked whether IFNγ-induced epithelial MHC class II expression is inhibited by CYT387 in *in vitro* organoid assays and found that CYT387 blunted the induction of MHC class II expression in response to IFNγ (Figure 5J). We also assessed the necessity of IFNγ signaling in regulating epithelial MHC class II expression by using IFNGR1 knockout (KO) mice and found dampened epithelial MHC class II expression in IFNGR1 knockout mice compared with wild-type controls (Figure 5K). The HFD-mediated reduction in IFNγ-inducible gene expression in ISCs suggests that intestinal immune cells may be depleted in the intestinal epithelium. We observed significant reduction of CD45+ immune infiltrates, such as CD3+, CD8+, and CD4+ T cells, involving the crypt epithelium (Figure S4). Altogether, these results suggest that PRR and IFNγ signaling drives MHC class II expression in the intestinal epithelial cells, including Lgr5+ ISCs, and that HFD feeding attenuates MHC class II expression in ISCs by suppressing these pathways and is in accordance with prior studies that demonstrated reduced inflammatory gene expression and immune infiltration in HFD intestinal crypts (Beyaz et al., 2016; Johnson et al., 2015; Schulz et al., 2014).

Dampening MHC class II expression in premalignant Lgr5+ ISCs increases intestinal tumorigenesis

Recognition of antigens by T cells through antigen presentation pathways is a key mechanism for triggering anti-tumor immunity

(F) *In situ* hybridization for *H2-Ab1* in vehicle- and JAK1/2 and TBK1/IKKε inhibitor (CYT387)-treated mice in small intestine (n = 3). Scale bars, 100 and 20 μm (insets).
(G) Relative expression of MHC class II (*H2-Ab1*) in Lgr5+ ISCs from vehicle- and CYT387-treated mice (n = 7, mean ± SEM).
(H and I) MFI of MHC class II in Lgr5+ ISCs from vehicle- and CYT387-treated mice (H) (n = 5, mean ± SEM). Representative flow cytometry histogram plots of MHC class II expression in Lgr5+ ISCs (I).
(J) Relative expression of MHC class II (*H2-Ab1*) in intestinal organoids treated with or without CYT387 and/or IFNγ (n = 5, mean ± SEM).
(K) Relative expression of MHC class II (*H2-Ab1*) in Epcam+ cells isolated from crypts of control or IFNGR1 KO (n = 5, mean ± SEM).
*p < 0.05, **p < 0.01, ***p < 0.001 (Student's t tests). See also Figures S3 and S4.

Please cite this article in press as: Beyaz et al., Dietary suppression of MHC class II expression in intestinal epithelial cells enhances intestinal tumorigenesis, Cell Stem Cell (2021), https://doi.org/10.1016/j.stem.2021.08.007

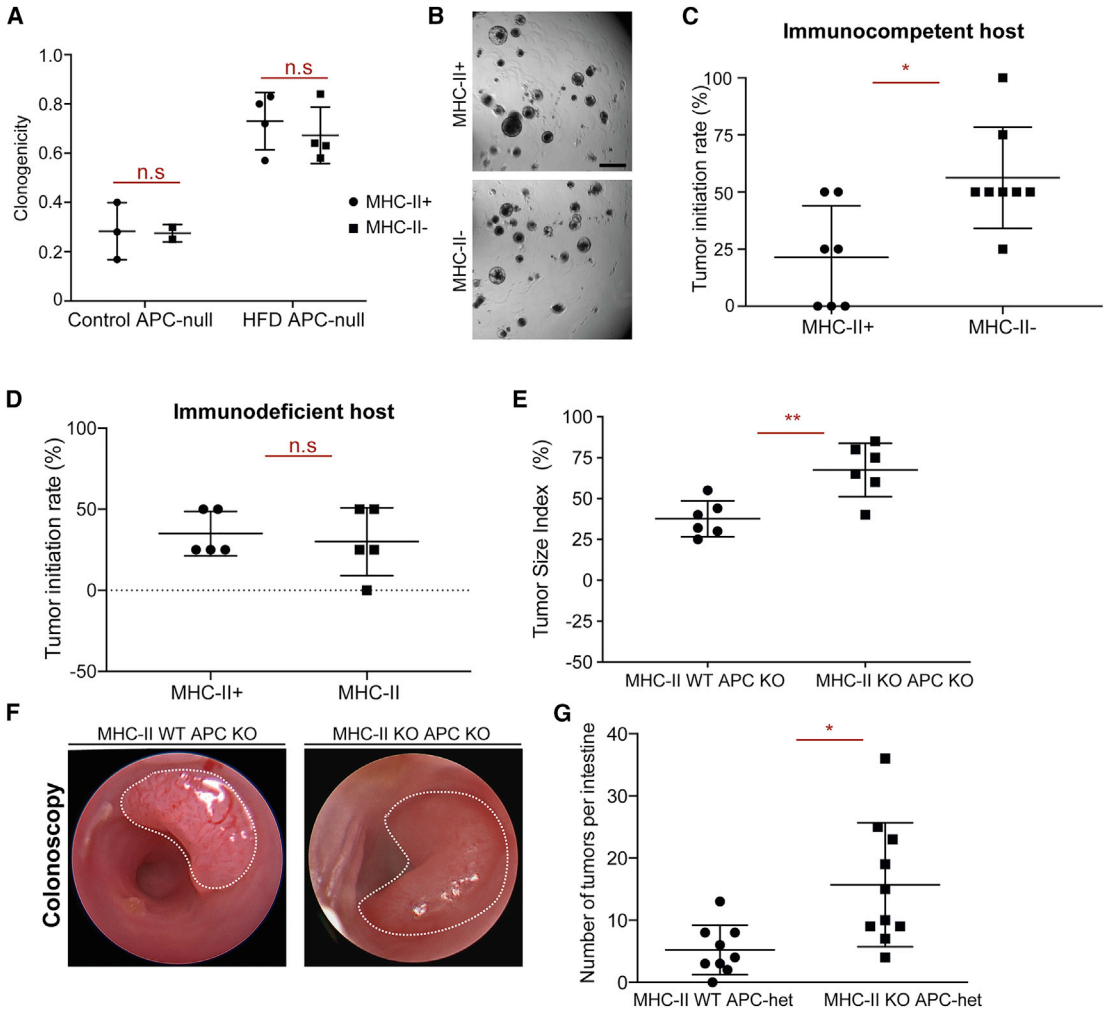

Figure 6. Loss of MHC class II in premalignant ISCs increases tumor initiation

(A and B) Organoid-initiating capacity of control and HFD *Apc*^{null} MHC-II+ and *Apc*^{null} MHC-II− Lgr5+ ISCs at day 5 (control MHC-II+, n = 3; control MHC-II−, n = 3; HFD MHC-II+, n = 4; HFD MHC-II−, n = 4; mean ± SD). Representative images of HFD *Apc*^{null} MHC-II+ and *Apc*^{null} MHC-II− organoids at day 5 (B). Scale bar, 100 μm (B).

(C) Tumor initiation rate of orthotopically transplanted *Apc*^{null} MHC-II+ and *Apc*^{null} MHC-II− Lgr5+ ISCs from HFD mice into immunocompetent syngeneic hosts (n = 8).

(D) Tumor initiation rate of orthotopically transplanted *Apc*^{null} MHC-II+ *Apc*^{null} and MHC-II− Lgr5+ ISCs from HFD mice into immunodeficient (Rag2 KO) hosts (n = 8).

(E and F) Tumor size index in the distal colon of mice that received tamoxifen through endoscopy-guided tamoxifen injection to induce tumor formation upon loss of APC (E) (n = 6; MHC-II WT APC KO, villin-Cre-ERT2 APC$^{L/L}$, MHC-II$^{L/+}$; MHC-II KO APC KO, villin-Cre-ERT2 APC$^{L/L}$, MHC-II$^{L/L}$). Representative optical colonoscopy images of tumors (F).

(G) Number of tumors per small intestine in Lgr5-CreERT2 MHC-II$^{L/+}$, APC$^{L/+}$ (n = 9, MHC-II WT APC-het) and Lgr5-CreERT2 MHC-II$^{L/L}$, APC$^{L/+}$ (n = 9, MHC-II KO APC KO) mice 5 months after tamoxifen injection.

Unless otherwise indicated, data are mean ± SEM from n independent experiments; n.s., not significant; *p < 0.05; **p < 0.01 (Student's t tests). See also Figures S5 and S6.

(Vanneman and Dranoff, 2012). Dampening the expression of genes involved in antigen presentation to evade anti-tumor immune responses is a hallmark of many cancers and correlates with poor prognosis (Løvig et al., 2002; Rimsza et al., 2004; Tarafdar et al., 2017). To test whether MHC class II expression patterns influence the tumor initiation potential of premalignant Lgr5+ ISCs, we fed Lgr5-CreERT2;Apc$^{L/L}$ mice control diet or HFD diet before tamoxifen-induced inactivation of the *Apc* tumor suppressor gene (APC^{null}) in Lgr5+ ISCs. HFD led to strong downregulation of MHC class II in premalignant APC^{null} Lgr5+ ISCs at both RNA and protein levels compared with controls (Figures S5A and S5C). As we observed in the non-neoplastic intestine (Figures 2G and 2H), MHC class II expression levels of APC^{null} Lgr5+ ISCs did not influence their ability to form adenomatous organoids *in vitro* (Figures 6A and 6B), indicating that the cell-intrinsic oncogenic potential of premalignant APC^{null} ISCs in organoid cultures that lack immune cells is independent of MHC class II.

Please cite this article in press as: Beyaz et al., Dietary suppression of MHC class II expression in intestinal epithelial cells enhances intestinal tumorigenesis, Cell Stem Cell (2021), https://doi.org/10.1016/j.stem.2021.08.007

To decipher whether HFD-mediated reduction in MHC class II expression on APC^{null} Lgr5+ ISCs affects tumorigenesis *in vivo*, we used a recently developed orthotopic, syngeneic colon transplantation assay in mice (Beyaz et al., 2016; Roper et al., 2017, 2018). We sorted APC^{null} MHC-II+ or APC^{null} MHC-II− Lgr5+ ISCs by flow cytometry and transplanted these populations into the colonic mucosa/submucosa of syngeneic, immune-competent mice. In contrast to the *in vitro* organoid assay, APC^{null} MHC-II− Lgr5+ ISCs exhibited 2-fold greater tumorigenicity when transplanted *in vivo* than their APC^{null} MHC-II+ counterparts (Figures 6C and S5D–S5F). Remarkably, when transplanted into immunodeficient Rag2 null host colons that lack adaptive B and T immune cells, both APC^{null} MHC-II+ and APC^{null} MHC-II− premalignant cells gave rise to equal numbers of tumors, highlighting a critical role for MHC class II recognition by adaptive immune cells in controlling intestinal tumor initiation (Figures 6D and S5G–S5I). Finally, to ascertain the specific role that epithelial MHC class II plays during intestinal tumorigenesis, we generated two genetic mouse models. First, using epithelial-specific inducible deletion model of MHC class II, together with tumor suppressor *Apc* (villin-CreERT2; $Apc^{L/L}$; MHC-$II^{L/L}$), we initiated single tumors in the distal colon by administering 4-Hydroxytamoxifen (4-OHT) with our endoscopy-guided injection system. We found that mice with the MHC class II-deficient allele (MHC-II KO: villin-CreERT2; $APC^{L/L}$, MHC-$II^{L/L}$) engendered larger tumors compared with mice with the MHC-sufficient allele (WT: villin-CreERT2; $APC^{L/L}$, MHC-$II^{L/+}$) (Figures 6E and 6F). Second, we initiated tumors using an Lgr5+ ISC-specific inducible deletion model of MHC class II, together with one copy of the tumor suppressor *Apc* that leads to intestinal tumor formation because of loss of heterozygosity (Lgr5CreERT2; MHC-$II^{L/+ \text{ or } L/L}$; $APC^{L/+}$). We found that loss of MHC class II specifically in Lgr5+ ISCs and their progeny was associated with greater numbers of intestinal tumors compared with their MHC class II-proficient counterparts (Figures 6G and S5J–S5L). Furthermore, we found that intestine-specific deletion of *Apc* resulted in the exclusion of both CD4+ and CD8+ T cells from established tumors in both MHC class II-deficient and MHC class II-proficient settings (Figures S5M–S5O and S6A–S6E), as has been previously reported in tumors with Wnt/β-catenin pathway activation (Kettunen et al., 2003; Luke et al., 2019). Altogether, these results illustrate that HFD-mediated reduction or genetic inactivation of MHC class II expression in premalignant ISCs enhances tumor formation in the intestine.

DISCUSSION

Lgr5+ ISCs continuously self-renew and differentiate into cells that comprise the intestinal epithelium. (Clevers, 2013). Acquisition of oncogenic mutations in these rapidly cycling stem cells leads to tumors that are subject to clearance by T cells (Agudo et al., 2018; Barker et al., 2009; Schepers et al., 2012). Here, we find that a HFD dampens MHC class II expression in IECs and Lgr5+ ISCs, and the reduction in epithelial MHC class II expression promotes intestinal tumor initiation. Although MHC class I antigen presentation pathway-mediated activation of cytotoxic $CD8^+$ T cells is frequently studied in the context of anti-tumor immune responses, MHC class II-mediated activation of $CD4^+$ T cells is also pivotal for tumor immunity (Hung et al., 1998; Takeuchi and Saito, 2017; Tran et al., 2014; Wang, 2001; Xie et al., 2010; Zhang et al., 2009). Studies have demonstrated that MHC class II-restricted $CD4^+$ T cells are able to eradicate tumors both directly and indirectly through the licensing of dendritic cells and helping $CD8^+$ T cell responses (Haabeth et al., 2016; Haspot et al., 2014; Hirschhorn-Cymerman et al., 2012; Kreiter et al., 2015; Lu et al., 2017; Spitzer et al., 2017; Tran et al., 2014). Consistent with prior studies demonstrating that tumors downregulate MHC class II expression to escape immune surveillance (Park et al., 2017; Tarafdar et al., 2017), our data implicate dietary regulation of MHC class II expression in ISCs as playing a critical role in intestinal tumorigenesis. A large-scale, genome-wide variant scan for colorectal cancer identified variants associated with cancer risk in MHC class II gene loci (Huyghe et al., 2019). Whether HFD-induced suppression of MHC class II expression in ISCs affects tumor initiation directly by eliciting anti-tumor CD4+ T cell response or indirectly by regulating CD8+ T cell response warrants further investigation.

It is becoming increasingly evident that the crosstalk between tissue stem cells and immune cells influences differentiation, homeostasis, and cancer risk (Ali et al., 2017; Hoytema van Konijnenburg et al., 2017; Lindemans et al., 2015; Naik et al., 2017, 2018; Ordovas-Montanes et al., 2020). Together with recent studies, our findings establish a functional role for epithelial MHC class II expression in regulating epithelial-immune crosstalk in the intestine and tumorigenesis (Biton et al., 2018; Fu et al., 2019b; Koyama et al., 2019; Tuganbaev et al., 2020). Importantly, we find that the intestinal microbiome is a crucial mediator of the epithelial MHC class II expression through TLR2/Myd88 and IFNγ signaling within intestinal epithelial cells, which are perturbed in response to HFD. Among bacterial species depleted by HFD, abundance of *Helicobacter* spp. correlates with epithelial MHC class II expression. This observation is consistent with our previous report demonstrating that several gram-negative *Helicobacter* species activate TLR2 receptors in the intestine (Mandell et al., 2004). Altogether, our results highlight how diet affects the interactions of microbes, stem cells, and immune cells in the intestine and contributes to tumor initiation (Figure S6F). Because a HFD influences cancer incidence in both mucosal and non-mucosal tissues (Beyaz et al., 2016; Chen et al., 2018; Kroenke et al., 2013; Pascual et al., 2017; Schulz et al., 2014; Yang et al., 2008, 2017), it will be important to explore whether the MHC class II-mediated immune surveillance of stem cells takes place in other tissues and how dietary perturbations influence tissue homeostasis and tumorigenesis by altering epithelial MHC class II expression.

LIMITATIONS OF STUDY

Although our data indicate that loss of epithelial MHC class II expression enhances intestinal tumor initiation, the precise immune mechanisms that mediate this process require further investigations. Consistent with previous reports (Kettunen et al., 2003; Luke et al., 2019), our tumor initiation models that are driven by intestine-specific loss of *Apc* and enhanced Wnt/β-catenin pathway activity resulted in exclusion of both CD4+ and CD8+ T cells in established tumors, thus constituting a

limitation for delineating the specific roles that T cell subsets play during epithelial MHC class II-mediated regulation of intestinal tumor formation. Future studies are needed to address the significance of epithelial MHC class II-mediated antigen presentation in regulating T cell responses during the early steps of tumor formation in the intestine. In addition, the causal links between specific microbes and epithelial MHC class II expression in the context of tumorigenesis are not addressed in this study. Although we identified several microbes that correlate with epithelial MHC class II expression, it will be important to identify in future studies the precise mechanisms of how microbes such as *Helicobacter* and *Odoribacter* directly or indirectly influence epithelial MHC class II expression and control intestinal homeostasis and tumorigenesis in the intestine.

STAR★METHODS

Detailed methods are provided in the online version of this paper and include the following:

- KEY RESOURCES TABLE
- RESOURCE AVAILABILITY
  - Lead contact
  - Materials availability
  - Data and code availability
- EXPERIMENTAL MODEL AND SUBJECT DETAILS
  - Animals, diet, and drug treatment
- METHOD DETAILS
  - Immunohistochemistry (IHC)
  - *In situ* hybridization
  - Intestinal crypt isolation and flow cytometry
  - Organoid culture for crypts and isolated cells
  - DQ-Ovalbumin Assay
  - Bulk RNA-Seq Analysis
  - qRT-PCR
  - Single cell RNA-Seq
  - Taxonomic microbiota analysis
  - Endoscopy-guided orthotopic tumor transplantation and injections
- QUANTIFICATION AND STATISTICAL ANALYSIS

SUPPLEMENTAL INFORMATION

Supplemental information can be found online at https://doi.org/10.1016/j.stem.2021.08.007.

ACKNOWLEDGMENTS

We thank CSHL Cancer Center Shared Resources (Animal, Flow Cytometry and Histology Core Facilities), supported by NCI Cancer Center Support grant 5P30CA045508. We also thank the Whitehead Institute Flow Cytometry Core and the Koch Institute Flow Cytometry and Histology Core facilities (NCI P30-CA14051). S.B. is supported by the Oliver S. and Jennie R. Donaldson Charitable Trust, Mathers Foundation, STARR Cancer Consortium (I13-0052), Mark Foundation For Cancer Research (20-028-EDV), and NIH (P30CA045508-33). Ö.H.Y. is supported by the NIH (R01 CA211184, CA254314, DK126545, U01CA250554, and P30CA14051-43), MIT Stem Cell Initiative through Foundation MIT, and Pew Foundation. S.H.O. is supported by the Howard Hughes Medical Institute. M.F. is supported by the American Association of Immunologists through a Career Reentry Fellowship.

AUTHOR CONTRIBUTIONS

S.B. conceived, designed, performed, and interpreted all experiments with support from C.C., H.M., K.E.B.-R., M.E.X., and I.E. L.D., C.A.T., E.E., D.A., and J.G.F. provided resources and experimental and analytical support for microbiome studies. M.B., K.S., and A.R. performed and analyzed scRNA-seq. O.E., K.P., K.O., M.A., B.Y., M.F., E.V.-E., A.E., K.D., V.S., A.A.-G., and J.R. provided experimental support. H.V.M., D.M.Ö., and A.K. provided analytical support. J.R., P.K., and J.P.M. provided resources. S.B. wrote the manuscript with support from S.H.O. and Ö.H.Y., and all authors edited the manuscript.

DECLARATION OF INTERESTS

The authors declare no competing financial interests. S.H.O. serves as an advisory board member for *Cell Stem Cell*. S.B. received research funding from Elstar Therapeutics and Revitope Oncology for research that is not related to this study.

INCLUSION AND DIVERSITY

We worked to ensure sex balance in the selection of non-human subjects. One or more of the authors of this paper self-identifies as an underrepresented ethnic minority in science.

Received: October 19, 2020
Revised: May 25, 2021
Accepted: August 10, 2021
Published: September 10, 2021

REFERENCES

Abreu, M.T. (2010). Toll-like receptor signalling in the intestinal epithelium: how bacterial recognition shapes intestinal function. Nat. Rev. Immunol. *10*, 131–144.

Agudo, J., Park, E.S., Rose, S.A., Alibo, E., Sweeney, R., Dhainaut, M., Kobayashi, K.S., Sachidanandam, R., Baccarini, A., Merad, M., and Brown, B.D. (2018). Quiescent Tissue Stem Cells Evade Immune Surveillance. Immunity *48*, 271–285.e5.

Ali, N., Zirak, B., Rodriguez, R.S., Pauli, M.L., Truong, H.A., Lai, K., Ahn, R., Corbin, K., Lowe, M.M., Scharschmidt, T.C., et al. (2017). Regulatory T Cells in Skin Facilitate Epithelial Stem Cell Differentiation. Cell *169*, 1119–1129.e11.

Anders, S., and Huber, W. (2010). Differential expression analysis for sequence count data. Genome Biol. *11*, R106.

Barker, N., van Es, J.H., Kuipers, J., Kujala, P., van den Born, M., Cozijnsen, M., Haegebarth, A., Korving, J., Begthel, H., Peters, P.J., and Clevers, H. (2007). Identification of stem cells in small intestine and colon by marker gene Lgr5. Nature *449*, 1003–1007.

Barker, N., Ridgway, R.A., van Es, J.H., van de Wetering, M., Begthel, H., van den Born, M., Danenberg, E., Clarke, A.R., Sansom, O.J., and Clevers, H. (2009). Crypt stem cells as the cells-of-origin of intestinal cancer. Nature *457*, 608–611.

Barriga, F.M., Montagni, E., Mana, M., Mendez-Lago, M., Hernando-Momblona, X., Sevillano, M., Guillaumet-Adkins, A., Rodriguez-Esteban, G., Buczacki, S.J.A., Gut, M., et al. (2017). Mex3a Marks a Slowly Dividing Subpopulation of Lgr5+ Intestinal Stem Cells. Cell Stem Cell *20*, 801–816.e7.

Basen-Engquist, K., and Chang, M. (2011). Obesity and cancer risk: recent review and evidence. Curr. Oncol. Rep. *13*, 71–76.

Belkaid, Y., and Hand, T.W. (2014). Role of the microbiota in immunity and inflammation. Cell *157*, 121–141.

Beyaz, S., and Yilmaz, O.H. (2016). Molecular Pathways: Dietary Regulation of Stemness and Tumor Initiation by the PPAR-δ Pathway. Clin. Cancer Res. *22*, 5636–5641.

Beyaz, S., Mana, M.D., Roper, J., Kedrin, D., Saadatpour, A., Hong, S.J., Bauer-Rowe, K.E., Xifaras, M.E., Akkad, A., Arias, E., et al. (2016). High-fat diet enhances stemness and tumorigenicity of intestinal progenitors. Nature *531*, 53–58.

Beyaz, S., Kim, J.H., Pinello, L., Xifaras, M.E., Hu, Y., Huang, J., Kerenyi, M.A., Das, P.P., Barnitz, R.A., Herault, A., et al. (2017). The histone demethylase UTX regulates the lineage-specific epigenetic program of invariant natural killer T cells. Nat. Immunol. *18*, 184–195.

Beyaz, S., Mana, M.D., and Yilmaz, O.H. (2021). High-fat diet activates a PPAR-δ program to enhance intestinal stem cell function. Cell Stem Cell *28*, 598–599.

Biton, M., Haber, A.L., Rogel, N., Burgin, G., Beyaz, S., Schnell, A., Ashenberg, O., Su, C.W., Smillie, C., Shekhar, K., et al. (2018). T Helper Cell Cytokines Modulate Intestinal Stem Cell Renewal and Differentiation. Cell *175*, 1307–1320.e22.

Brown, M., Hughes, K.R., Moossavi, S., Robins, A., and Mahida, Y.R. (2014). Toll-like receptor expression in crypt epithelial cells, putative stem cells and intestinal myofibroblasts isolated from controls and patients with inflammatory bowel disease. Clin. Exp. Immunol. *178*, 28–39.

Calle, E.E., Rodriguez, C., Walker-Thurmond, K., and Thun, M.J. (2003). Overweight, obesity, and mortality from cancer in a prospectively studied cohort of U.S. adults. N. Engl. J. Med. *348*, 1625–1638.

Caruso, R., Warner, N., Inohara, N., and Núñez, G. (2014). NOD1 and NOD2: signaling, host defense, and inflammatory disease. Immunity *41*, 898–908.

Cerf-Bensussan, N., Quaroni, A., Kurnick, J.T., and Bhan, A.K. (1984). Intraepithelial lymphocytes modulate Ia expression by intestinal epithelial cells. J. Immunol. *132*, 2244–2252.

Chen, M., Zhang, J., Sampieri, K., Clohessy, J.G., Mendez, L., Gonzalez-Billalabeitia, E., Liu, X.S., Lee, Y.R., Fung, J., Katon, J.M., et al. (2018). An aberrant SREBP-dependent lipogenic program promotes metastatic prostate cancer. Nat. Genet. *50*, 206–218.

Choi, N.M., Majumder, P., and Boss, J.M. (2011). Regulation of major histocompatibility complex class II genes. Curr. Opin. Immunol. *23*, 81–87.

Clevers, H. (2013). The intestinal crypt, a prototype stem cell compartment. Cell *154*, 274–284.

Coleman, D.L. (1978). Obese and diabetes: two mutant genes causing diabetes-obesity syndromes in mice. Diabetologia *14*, 141–148.

Collins, T., Korman, A.J., Wake, C.T., Boss, J.M., Kappes, D.J., Fiers, W., Ault, K.A., Gimbrone, M.A., Jr., Strominger, J.L., and Pober, J.S. (1984). Immune interferon activates multiple class II major histocompatibility complex genes and the associated invariant chain gene in human endothelial cells and dermal fibroblasts. Proc. Natl. Acad. Sci. USA *81*, 4917–4921.

Colnot, S., Niwa-Kawakita, M., Hamard, G., Godard, C., Le Plenier, S., Houbron, C., Romagnolo, B., Berrebi, D., Giovannini, M., and Perret, C. (2004). Colorectal cancers in a new mouse model of familial adenomatous polyposis: influence of genetic and environmental modifiers. Lab. Invest. *84*, 1619–1630.

Dahan, S., Roth-Walter, F., Arnaboldi, P., Agarwal, S., and Mayer, L. (2007). Epithelia: lymphocyte interactions in the gut. Immunol. Rev. *215*, 243–253.

David, L.A., Maurice, C.F., Carmody, R.N., Gootenberg, D.B., Button, J.E., Wolfe, B.E., Ling, A.V., Devlin, A.S., Varma, Y., Fischbach, M.A., et al. (2014). Diet rapidly and reproducibly alters the human gut microbiome. Nature *505*, 559–563.

Dong, C., Juedes, A.E., Temann, U.A., Shresta, S., Allison, J.P., Ruddle, N.H., and Flavell, R.A. (2001). ICOS co-stimulatory receptor is essential for T-cell activation and function. Nature *409*, 97–101.

Finak, G., McDavid, A., Yajima, M., Deng, J., Gersuk, V., Shalek, A.K., Slichter, C.K., Miller, H.W., McElrath, M.J., Prlic, M., et al. (2015). MAST: a flexible statistical framework for assessing transcriptional changes and characterizing heterogeneity in single-cell RNA sequencing data. Genome Biol. *16*, 278.

Font-Burgada, J., Sun, B., and Karin, M. (2016). Obesity and Cancer: The Oil that Feeds the Flame. Cell Metab. *23*, 48–62.

Fu, T., Coulter, S., Yoshihara, E., Oh, T.G., Fang, S., Cayabyab, F., Zhu, Q., Zhang, T., Leblanc, M., Liu, S., et al. (2019a). FXR Regulates Intestinal Cancer Stem Cell Proliferation. Cell *176*, 1098–1112.e18.

Fu, Y.Y., Egorova, A., Sobieski, C., Kuttiyara, J., Calafiore, M., Takashima, S., Clevers, H., and Hanash, A.M. (2019b). T Cell Recruitment to the Intestinal Stem Cell Compartment Drives Immune-Mediated Intestinal Damage after Allogeneic Transplantation. Immunity *51*, 90–103.e3.

Gallagher, E.J., and LeRoith, D. (2015). Obesity and Diabetes: The Increased Risk of Cancer and Cancer-Related Mortality. Physiol. Rev. *95*, 727–748.

Grasso, C.S., Giannakis, M., Wells, D.K., Hamada, T., Mu, X.J., Quist, M., Nowak, J.A., Nishihara, R., Qian, Z.R., Inamura, K., et al. (2018). Genetic Mechanisms of Immune Evasion in Colorectal Cancer. Cancer Discov. *8*, 730–749.

Haabeth, O.A., Tveita, A., Fauskanger, M., Hennig, K., Hofgaard, P.O., and Bogen, B. (2016). Idiotype-specific CD4(+) T cells eradicate disseminated myeloma. Leukemia *30*, 1216–1220.

Haspot, F., Li, H.W., Lucas, C.L., Fehr, T., Beyaz, S., and Sykes, M. (2014). Allospecific rejection of MHC class I-deficient bone marrow by CD8 T cells. Am. J. Transplant. *14*, 49–58.

Hershberg, R.M., Framson, P.E., Cho, D.H., Lee, L.Y., Kovats, S., Beitz, J., Blum, J.S., and Nepom, G.T. (1997). Intestinal epithelial cells use two distinct pathways for HLA class II antigen processing. J. Clin. Invest. *100*, 204–215.

Hirschhorn-Cymerman, D., Budhu, S., Kitano, S., Liu, C., Zhao, F., Zhong, H., Lesokhin, A.M., Avogadri-Connors, F., Yuan, J., Li, Y., et al. (2012). Induction of tumoricidal function in CD4+ T cells is associated with concomitant memory and terminally differentiated phenotype. J. Exp. Med. *209*, 2113–2126.

Hooper, L.V., Littman, D.R., and Macpherson, A.J. (2012). Interactions between the microbiota and the immune system. Science *336*, 1268–1273.

Howie, D., Garcia Rueda, H., Brown, M.H., and Waldmann, H. (2013). Secreted and transmembrane 1A is a novel co-stimulatory ligand. PLoS ONE *8*, e73610.

Hoytema van Konijnenburg, D.P., Reis, B.S., Pedicord, V.A., Farache, J., Victora, G.D., and Mucida, D. (2017). Intestinal Epithelial and Intraepithelial T Cell Crosstalk Mediates a Dynamic Response to Infection. Cell *171*, 783–794.e13.

Hung, K., Hayashi, R., Lafond-Walker, A., Lowenstein, C., Pardoll, D., and Levitsky, H. (1998). The central role of CD4(+) T cells in the antitumor immune response. J. Exp. Med. *188*, 2357–2368.

Huyghe, J.R., Bien, S.A., Harrison, T.A., Kang, H.M., Chen, S., Schmit, S.L., Conti, D.V., Qu, C., Jeon, J., Edlund, C.K., et al. (2019). Discovery of common and rare genetic risk variants for colorectal cancer. Nat. Genet. *51*, 76–87.

Johnson, A.M., Costanzo, A., Gareau, M.G., Armando, A.M., Quehenberger, O., Jameson, J.M., and Olefsky, J.M. (2015). High fat diet causes depletion of intestinal eosinophils associated with intestinal permeability. PLoS ONE *10*, e0122195.

Kettunen, H.L., Kettunen, A.S., and Rautonen, N.E. (2003). Intestinal immune responses in wild-type and Apcmin/+ mouse, a model for colon cancer. Cancer Res. *63*, 5136–5142.

Koyama, M., Mukhopadhyay, P., Schuster, I.S., Henden, A.S., Hülsdünker, J., Varelias, A., Vetizou, M., Kuns, R.D., Robb, R.J., Zhang, P., et al. (2019). MHC Class II Antigen Presentation by the Intestinal Epithelium Initiates Graft-versus-Host Disease and Is Influenced by the Microbiota. Immunity *51*, 885–898.e7.

Kreiter, S., Vormehr, M., van de Roemer, N., Diken, M., Löwer, M., Diekmann, J., Boegel, S., Schrörs, B., Vascotto, F., Castle, J.C., et al. (2015). Mutant MHC class II epitopes drive therapeutic immune responses to cancer. Nature *520*, 692–696.

Kroenke, C.H., Kwan, M.L., Sweeney, C., Castillo, A., and Caan, B.J. (2013). High- and low-fat dairy intake, recurrence, and mortality after breast cancer diagnosis. J. Natl. Cancer Inst. *105*, 616–623.

Kucukural, A., Yukselen, O., Ozata, D.M., Moore, M.J., and Garber, M. (2019). DEBrowser: interactive differential expression analysis and visualization tool for count data. BMC Genomics *20*, 6.

Langmead, B., and Salzberg, S.L. (2012). Fast gapped-read alignment with Bowtie 2. Nat Methods *9*, 357–359.

Ley, R.E., Bäckhed, F., Turnbaugh, P., Lozupone, C.A., Knight, R.D., and Gordon, J.I. (2005). Obesity alters gut microbial ecology. Proc. Natl. Acad. Sci. USA *102*, 11070–11075.

Li, B., and Dewey, C.N. (2011). RSEM: accurate transcript quantification from RNA-Seq data with or without a reference genome. BMC Bioinformatics *12*, 323.

Li, W., Zimmerman, S.E., Peregrina, K., Houston, M., Mayoral, J., Zhang, J., Maqbool, S., Zhang, Z., Cai, Y., Ye, K., and Augenlicht, L.H. (2019). The nutritional environment determines which and how intestinal stem cells contribute to homeostasis and tumorigenesis. Carcinogenesis *40*, 937–946.

Lindemans, C.A., Calafiore, M., Mertelsmann, A.M., O'Connor, M.H., Dudakov, J.A., Jenq, R.R., Velardi, E., Young, L.F., Smith, O.M., Lawrence, G., et al. (2015). Interleukin-22 promotes intestinal-stem-cell-mediated epithelial regeneration. Nature *528*, 560–564.

Liu, L., Nishihara, R., Qian, Z.R., Tabung, F.K., Nevo, D., Zhang, X., Song, M., Cao, Y., Mima, K., Masugi, Y., et al. (2017). Association Between Inflammatory Diet Pattern and Risk of Colorectal Carcinoma Subtypes Classified by Immune Responses to Tumor. Gastroenterology *153*, 1517–1530.

Løvig, T., Andersen, S.N., Thorstensen, L., Diep, C.B., Meling, G.I., Lothe, R.A., and Rognum, T.O. (2002). Strong HLA-DR expression in microsatellite stable carcinomas of the large bowel is associated with good prognosis. Br. J. Cancer *87*, 756–762.

Lu, Y.C., Parker, L.L., Lu, T., Zheng, Z., Toomey, M.A., White, D.E., Yao, X., Li, Y.F., Robbins, P.F., Feldman, S.A., et al. (2017). Treatment of Patients With Metastatic Cancer Using a Major Histocompatibility Complex Class II-Restricted T-Cell Receptor Targeting the Cancer Germline Antigen MAGE-A3. J. Clin. Oncol. *35*, 3322–3329.

Luke, J.J., Bao, R., Sweis, R.F., Spranger, S., and Gajewski, T.F. (2019). WNT/β-catenin Pathway Activation Correlates with Immune Exclusion across Human Cancers. Clin. Cancer Res. *25*, 3074–3083.

Mandell, L., Moran, A.P., Cocchiarella, A., Houghton, J., Taylor, N., Fox, J.G., Wang, T.C., and Kurt-Jones, E.A. (2004). Intact gram-negative *Helicobacter pylori*, *Helicobacter felis*, and *Helicobacter hepaticus* bacteria activate innate immunity via toll-like receptor 2 but not toll-like receptor 4. Infect. Immun. *72*, 6446–6454.

Mukherjee, S., and Hooper, L.V. (2015). Antimicrobial defense of the intestine. Immunity *42*, 28–39.

Naik, S., Larsen, S.B., Gomez, N.C., Alaverdyan, K., Sendoel, A., Yuan, S., Polak, L., Kulukian, A., Chai, S., and Fuchs, E. (2017). Inflammatory memory sensitizes skin epithelial stem cells to tissue damage. Nature *550*, 475–480.

Naik, S., Larsen, S.B., Cowley, C.J., and Fuchs, E. (2018). Two to Tango: Dialog between Immunity and Stem Cells in Health and Disease. Cell *175*, 908–920.

Neal, M.D., Sodhi, C.P., Jia, H., Dyer, M., Egan, C.E., Yazji, I., Good, M., Afrazi, A., Marino, R., Slagle, D., et al. (2012). Toll-like receptor 4 is expressed on intestinal stem cells and regulates their proliferation and apoptosis via the p53 up-regulated modulator of apoptosis. J. Biol. Chem. *287*, 37296–37308.

Ordovas-Montanes, J., Beyaz, S., Rakoff-Nahoum, S., and Shalek, A.K. (2020). Distribution and storage of inflammatory memory in barrier tissues. Nat. Rev. Immunol. *20*, 308–320.

Park, I.A., Hwang, S.H., Song, I.H., Heo, S.H., Kim, Y.A., Bang, W.S., Park, H.S., Lee, M., Gong, G., and Lee, H.J. (2017). Expression of the MHC class II in triple-negative breast cancer is associated with tumor-infiltrating lymphocytes and interferon signaling. PLoS ONE *12*, e0182786.

Pascual, G., Avgustinova, A., Mejetta, S., Martín, M., Castellanos, A., Attolini, C.S., Berenguer, A., Prats, N., Toll, A., Hueto, J.A., et al. (2017). Targeting metastasis-initiating cells through the fatty acid receptor CD36. Nature *541*, 41–45.

Pavot, V., Rochereau, N., Rességuier, J., Gutjahr, A., Genin, C., Tiraby, G., Perouzel, E., Lioux, T., Vernejoul, F., Verrier, B., and Paul, S. (2014). Cutting edge: New chimeric NOD2/TLR2 adjuvant drastically increases vaccine immunogenicity. J. Immunol. *193*, 5781–5785.

Picelli, S., Faridani, O.R., Bjorklund, A.K., Winberg, G., Sagasser, S., and Sandberg, R. (2014). Full-length RNA-seq from single cells using Smart-seq2. Nat Protoc *9*, 171–181.

Price, A.E., Shamardani, K., Lugo, K.A., Deguine, J., Roberts, A.W., Lee, B.L., and Barton, G.M. (2018). A Map of Toll-like Receptor Expression in the Intestinal Epithelium Reveals Distinct Spatial, Cell Type-Specific, and Temporal Patterns. Immunity *49*, 560–575.e6.

Rakoff-Nahoum, S., Paglino, J., Eslami-Varzaneh, F., Edberg, S., and Medzhitov, R. (2004). Recognition of commensal microflora by toll-like receptors is required for intestinal homeostasis. Cell *118*, 229–241.

Rimsza, L.M., Roberts, R.A., Miller, T.P., Unger, J.M., LeBlanc, M., Braziel, R.M., Weisenberger, D.D., Chan, W.C., Muller-Hermelink, H.K., Jaffe, E.S., et al. (2004). Loss of MHC class II gene and protein expression in diffuse large B-cell lymphoma is related to decreased tumor immunosurveillance and poor patient survival regardless of other prognostic factors: a follow-up study from the Leukemia and Lymphoma Molecular Profiling Project. Blood *103*, 4251–4258.

Roper, J., Richardson, M.P., Wang, W.V., Richard, L.G., Chen, W., Coffee, E.M., Sinnamon, M.J., Lee, L., Chen, P.C., Bronson, R.T., et al. (2011). The dual PI3K/mTOR inhibitor NVP-BEZ235 induces tumor regression in a genetically engineered mouse model of PIK3CA wild-type colorectal cancer. PLoS ONE *6*, e25132.

Roper, J., Tammela, T., Cetinbas, N.M., Akkad, A., Roghanian, A., Rickelt, S., Almeqdadi, M., Wu, K., Oberli, M.A., Sánchez-Rivera, F.J., et al. (2017). *In vivo* genome editing and organoid transplantation models of colorectal cancer and metastasis. Nat. Biotechnol. *35*, 569–576.

Roper, J., Tammela, T., Akkad, A., Almeqdadi, M., Santos, S.B., Jacks, T., and Yilmaz, O.H. (2018). Colonoscopy-based colorectal cancer modeling in mice with CRISPR-Cas9 genome editing and organoid transplantation. Nat. Protoc. *13*, 217–234.

Round, J.L., and Mazmanian, S.K. (2009). The gut microbiota shapes intestinal immune responses during health and disease. Nat. Rev. Immunol. *9*, 313–323.

Sade-Feldman, M., Jiao, Y.J., Chen, J.H., Rooney, M.S., Barzily-Rokni, M., Eliane, J.P., Bjorgaard, S.L., Hammond, M.R., Vitzthum, H., Blackmon, S.M., et al. (2017). Resistance to checkpoint blockade therapy through inactivation of antigen presentation. Nat. Commun. *8*, 1136.

Sato, T., Vries, R.G., Snippert, H.J., van de Wetering, M., Barker, N., Stange, D.E., van Es, J.H., Abo, A., Kujala, P., Peters, P.J., and Clevers, H. (2009). Single Lgr5 stem cells build crypt-villus structures *in vitro* without a mesenchymal niche. Nature *459*, 262–265.

Schepers, A.G., Snippert, H.J., Stange, D.E., van den Born, M., van Es, J.H., van de Wetering, M., and Clevers, H. (2012). Lineage tracing reveals Lgr5+ stem cell activity in mouse intestinal adenomas. Science *337*, 730–735.

Schulz, M.D., Atay, C., Heringer, J., Romrig, F.K., Schwitalla, S., Aydin, B., Ziegler, P.K., Varga, J., Reindl, W., Pommerenke, C., et al. (2014). High-fat-diet-mediated dysbiosis promotes intestinal carcinogenesis independently of obesity. Nature *514*, 508–512.

Shekhar, K., Lapan, S.W., Whitney, I.E., Tran, N.M., Macosko, E.Z., Kowalczyk, M., Adiconis, X., Levin, J.Z., Nemesh, J., Goldman, M., et al. (2016). Comprehensive Classification of Retinal Bipolar Neurons by Single-Cell Transcriptomics. Cell *166*, 1308–1323.e30.

Spitzer, M.H., Carmi, Y., Reticker-Flynn, N.E., Kwek, S.S., Madhireddy, D., Martins, M.M., Gherardini, P.F., Prestwood, T.R., Chabon, J., Bendall, S.C., et al. (2017). Systemic Immunity Is Required for Effective Cancer Immunotherapy. Cell *168*, 487–502.e15.

Takeuchi, A., and Saito, T. (2017). CD4 CTL, a Cytotoxic Subset of $CD4^+$ T Cells, Their Differentiation and Function. Front. Immunol. *8*, 194.

Tarafdar, A., Hopcroft, L.E., Gallipoli, P., Pellicano, F., Cassels, J., Hair, A., Korfi, K., Jørgensen, H.G., Vetrie, D., Holyoake, T.L., and Michie, A.M. (2017). CML cells actively evade host immune surveillance through cytokine-mediated downregulation of MHC-II expression. Blood *129*, 199–208.

Telega, G.W., Baumgart, D.C., and Carding, S.R. (2000). Uptake and presentation of antigen to T cells by primary colonic epithelial cells in normal and diseased states. Gastroenterology *119*, 1548–1559.

Thaiss, C.A., Itav, S., Rothschild, D., Meijer, M.T., Levy, M., Moresi, C., Dohnalová, L., Braverman, S., Rozin, S., Malitsky, S., et al. (2016). Persistent microbiome alterations modulate the rate of post-dieting weight regain. Nature *540*, 544–551.

Thelemann, C., Eren, R.O., Coutaz, M., Brasseit, J., Bouzourene, H., Rosa, M., Duval, A., Lavanchy, C., Mack, V., Mueller, C., et al. (2014). Interferon-γ

induces expression of MHC class II on intestinal epithelial cells and protects mice from colitis. PLoS ONE *9*, e86844.

Tomas, J., Mulet, C., Saffarian, A., Cavin, J.B., Ducroc, R., Regnault, B., Kun Tan, C., Duszka, K., Burcelin, R., Wahli, W., et al. (2016). High-fat diet modifies the PPAR-γ pathway leading to disruption of microbial and physiological ecosystem in murine small intestine. Proc. Natl. Acad. Sci. USA *113*, E5934–E5943.

Tran, E., Turcotte, S., Gros, A., Robbins, P.F., Lu, Y.C., Dudley, M.E., Wunderlich, J.R., Somerville, R.P., Hogan, K., Hinrichs, C.S., et al. (2014). Cancer immunotherapy based on mutation-specific CD4+ T cells in a patient with epithelial cancer. Science *344*, 641–645.

Trapnell, C., Pachter, L., and Salzberg, S.L. (2009). TopHat: discovering splice junctions with RNA-Seq. Bioinformatics *25*, 1105–1111.

Tuganbaev, T., Mor, U., Bashiardes, S., Liwinski, T., Nobs, S.P., Leshem, A., Dori-Bachash, M., Thaiss, C.A., Pinker, E.Y., Ratiner, K., et al. (2020). Diet Diurnally Regulates Small Intestinal Microbiome-Epithelial-Immune Homeostasis and Enteritis. Cell *182*, 1441–1459.e21.

Tyner, J.W., Bumm, T.G., Deininger, J., Wood, L., Aichberger, K.J., Loriaux, M.M., Druker, B.J., Burns, C.J., Fantino, E., and Deininger, M.W. (2010). CYT387, a novel JAK2 inhibitor, induces hematologic responses and normalizes inflammatory cytokines in murine myeloproliferative neoplasms. Blood *115*, 5232–5240.

van den Elsen, P.J. (2011). Expression regulation of major histocompatibility complex class I and class II encoding genes. Front. Immunol. *2*, 48.

Vanneman, M., and Dranoff, G. (2012). Combining immunotherapy and targeted therapies in cancer treatment. Nat. Rev. Cancer *12*, 237–251.

Wang, R.F. (2001). The role of MHC class II-restricted tumor antigens and CD4+ T cells in antitumor immunity. Trends Immunol. *22*, 269–276.

Wang, B., Rong, X., Palladino, E.N.D., Wang, J., Fogelman, A.M., Martín, M.G., Alrefai, W.A., Ford, D.A., and Tontonoz, P. (2018). Phospholipid Remodeling and Cholesterol Availability Regulate Intestinal Stemness and Tumorigenesis. Cell Stem Cell *22*, 206–220.e4.

Westendorf, A.M., Fleissner, D., Groebe, L., Jung, S., Gruber, A.D., Hansen, W., and Buer, J. (2009). CD4+Foxp3+ regulatory T cell expansion induced by antigen-driven interaction with intestinal epithelial cells independent of local dendritic cells. Gut *58*, 211–219.

Wong, G.H., Bartlett, P.F., Clark-Lewis, I., Battye, F., and Schrader, J.W. (1984). Inducible expression of H-2 and Ia antigens on brain cells. Nature *310*, 688–691.

Xie, Y., Akpinarli, A., Maris, C., Hipkiss, E.L., Lane, M., Kwon, E.K., Muranski, P., Restifo, N.P., and Antony, P.A. (2010). Naive tumor-specific CD4(+) T cells differentiated *in vivo* eradicate established melanoma. J. Exp. Med. *207*, 651–667.

Yang, K., Kurihara, N., Fan, K., Newmark, H., Rigas, B., Bancroft, L., Corner, G., Livote, E., Lesser, M., Edelmann, W., et al. (2008). Dietary induction of colonic tumors in a mouse model of sporadic colon cancer. Cancer Res. *68*, 7803–7810.

Yang, J.J., Yu, D., Takata, Y., Smith-Warner, S.A., Blot, W., White, E., Robien, K., Park, Y., Xiang, Y.B., Sinha, R., et al. (2017). Dietary Fat Intake and Lung Cancer Risk: A Pooled Analysis. J. Clin. Oncol. *35*, 3055–3064.

Yilmaz, O.H., Katajisto, P., Lamming, D.W., Gültekin, Y., Bauer-Rowe, K.E., Sengupta, S., Birsoy, K., Dursun, A., Yilmaz, V.O., Selig, M., et al. (2012). mTORC1 in the Paneth cell niche couples intestinal stem-cell function to calorie intake. Nature *486*, 490–495.

Yukselen, O., Turkyilmaz, O., Ozturk, A.R., Garber, M., and Kucukural, A. (2020). DolphinNext: a distributed data processing platform for high throughput genomics. BMC Genomics *21*, 310.

Zhang, S., Zhang, H., and Zhao, J. (2009). The role of CD4 T cell help for CD8 CTL activation. Biochem. Biophys. Res. Commun. *384*, 405–408.

Zitvogel, L., Pietrocola, F., and Kroemer, G. (2017). Nutrition, inflammation and cancer. Nat. Immunol. *18*, 843–850.

Please cite this article in press as: Beyaz et al., Dietary suppression of MHC class II expression in intestinal epithelial cells enhances intestinal tumorigenesis, Cell Stem Cell (2021), https://doi.org/10.1016/j.stem.2021.08.007

CellPress

STAR★METHODS

KEY RESOURCES TABLE

REAGENT or RESOURCE	SOURCE	IDENTIFIER
Antibodies		
Chicken anti-β-galactosidase	Abcam	ab9361, RRID: AB_307210
Rat anti-BrdU	Abcam	ab6326, RRID: AB_305426
Mouse anti-β catenin	BD Biosciences	610154, RRID: AB_397555
Rat anti-CD3ε, clone 145-2C11	Biolegend	100302, RRID: AB_312667
Rat anti-CD4, clone H129.19	Biolegend	130302, RRID: AB_1279242
Rat anti-CD8a, clone 53-6.7	Biolegend	100702, RRID: AB_312741
CD45-PE, clone 30-F11	eBioscience	12-0451-83, RRID: AB_465669
CD24-Pacfic Blue, clone M1/69	Biolegend	101820, RRID: AB_572011
EpCAM Apc, clone G8.8	eBioscience	17-5791-82, RRID: AB_2716944
PE I-A/I-E, clone M5/114.15.2	Biolegend	107608, RRID: AB_313323
7-AAD	Thermo Fisher	A1310
Anti-Ki67 (SP6)	Thermo Fisher	MA5-14520, RRID: AB_10979488
CD3e (D4V8L) rabbit monoclonal antibody	CST	99940, RRID: AB_2755035
CD8a (D4W2Z) rabbit monoclonal antibody	CST	98941, RRID: AB_2756376
CD3 FITC, clone 145-2C11	Biolegend	100306, RRID: AB_312671
CD4 PE-Cy7, clone GK1.5	Biolegend	100422, RRID: AB_312707
CD8a APC-Cy7, clone 53-6.7	Biolegend	100714, RRID: AB_312753
Chemicals, peptides, and recombinant proteins		
CYT387	Selleckchem	S2219
CL429	InvivoGen	tlrl-c429
GW501516	Enzo	ALX-420-032
DQ-ovalbumin	Thermo Fisher	D12053
Ifng	Peprotech	315-05
5-Bromo-2′-deoxyuridine	Sigma Aldrich	19-160
Metronidazole	Sigma Aldrich	M3761
Vancomycin	Sigma Aldrich	V2002
Ampicillin	Sigma Aldrich	A9518
Neomycin	Sigma Aldrich	N1142
PEG400	Sigma Aldrich	P4338
Tween-80	Sigma Aldrich	P4780
Tamoxifen	Sigma Aldrich	T5648
Sunflower Seed Oil	Spectrum	S1929
Matrigel	Corning	356231
Advanced DMEM	GIBCO	12491015
EGF	Peprotech	315-09
Noggin	Peprotech	250-38
R-spondin	Peprotech	315-32
N-acetyl-l-cystine	Sigma Aldrich	A9165
B27	Life Technologies	17504044
Chir99021 dihydrochloride	LC Laboratories	C-6556
Y-27632	Sigma Aldrich	Y0503
TrypLE Express Enzyme	Thermo Fisher	12604013
48 well plates	Olympus	25-108

(*Continued on next page*)

Please cite this article in press as: Beyaz et al., Dietary suppression of MHC class II expression in intestinal epithelial cells enhances intestinal tumorigenesis, Cell Stem Cell (2021), https://doi.org/10.1016/j.stem.2021.08.007

Continued

REAGENT or RESOURCE	SOURCE	IDENTIFIER
96 well plates	Olympus	25-109
JAG-1	Anaspec	AS-61298
TRI Reagent	Sigma Aldrich	93289
Critical commercial assays		
Elite ABC HRP Kit	Vector Laboratories	PK6100
Signalstain® DAB Substrate Kit	CST	8049S
Signalstain® Antibody Diluent	CST	8112L
RNAscope 2.0 HD Detection Kit	ACD RNAscope®	323110
RNAscope probe: *Mm-H2-Ab1*	ACD RNAscope®	Ref#414731
qScript cDNA SuperMix	Quantabio	95048
PerfeCTa SYBR green fast mix	Quantabio	95072
Deposited data		
Bulk RNA sequencing data	Beyaz et al., 2016	GEO: GSE67324
scRNA sequencing data	This study	GEO: GSE180949
Experimental models: Mouse		
$MHC^{L/L}$	The Jackson Laboratory	013181, RRID: IMSR_JAX:013181
Villin-CreERT2	Dr. Sylvie Robine	N/A
Lgr5-EGFP-IRES-CreERT2	The Jackson Laboratory	008875, RRID: IMSR_JAX:008875
Rosa26-LSL-lacZ	The Jackson Laboratory	003474, RRID: IMSR_JAX:003474
$APC^{L/L}$	Dr. Raju Kucherplati	N/A
Db/Db	The Jackson Laboratory	000697, RRID: IMSR_JAX:000697
IFNGR1 KO	The Jackson Laboratory	025545, RRID: IMSR_JAX:025545
$Myd88^{L/L}$	The Jackson Laboratory	008888, RRID: IMSR_JAX:008888
Villin-Cre	The Jackson Laboratory	021504, RRID: IMSR_JAX:021504
Lgr5-EGFP-IRES-CreERT2; $MHC^{L/L}$; $APC^{L/L}$	First presented in this work	N/A
Lgr5-EGFP-IRES-CreERT2; $MHC^{L/L}$; $APC^{L/+}$	First presented in this work	N/A
Villin-CreERT2; $MHC^{L/L}$; $APC^{L/L}$;	First presented in this work	N/A
Lgr5-EGFP-IRES-CreERT2, Rosa26-LSL-lacZ; $MHC^{L/L}$	First presented in this work	N/A
Mouse diets		
Control Diet	Research Diets	D12450J
High Fat Diet	Research Diets	D12492
Software and algorithms		
FlowJo v10.	FlowJo LLC	https://www.flowjo.com/
GraphPad Prism 8	GraphPad Software	https://www.graphpad.com/scientific-software/prism/
Aperio	Leica Biosystems	https://www.leicabiosystems.com
ImageJ-Fiji	NIH	https://fiji.sc/
Oligonucleotides		
Primers for qRT-PCR, see Table S3	IDT	N/A

RESOURCE AVAILABILITY

Lead contact

Further information and requests for resources and reagents should be directed to and will be fulfilled by Semir Beyaz (beyaz@cshl.edu).

Materials availability

All in-house generated mouse strains generated for this study are available from the Lead Contact with a completed Materials Transfer Agreement.

Data and code availability

RNA-seq and scRNA-seq data that are used in this study are available at Gene Expression Omnibus (GEO) with the following accession numbers GSE67324 and GSE180949.

EXPERIMENTAL MODEL AND SUBJECT DETAILS

Animals, diet, and drug treatment

The following strains were obtained from the Jackson Laboratory: *Lgr5-EGFP-IRES-CreERT2* (Lgr5-CreERT2) (strain name: B6.129P2-Lgr5$^{tm1(cre/ERT2)Cle}$/J, stock number 008875), *Rosa26-lacZ* (strain name: B6.129S4-Gt(ROSA)26Sor^{tm1Sor}/J, stock number 003474), *db/db* (strain name: B6.BKS(D)-Lepr^{jb}/J, stock number 000697), *Mhc*$^{L/L}$ (strain name: B6.129X1-H2-Ab1^{tm1Koni}/J, stock number 013181), IFNGR1 KO (C57BL/6N-Ifngr1tm1.2Rds/J, stock number 025545), Villin-Cre (B6.Cg-Tg(Vil1-cre)1000Gum/J Stock No: 021504), Myd88$^{L/L}$ (B6.129P2(SJL)-Myd88tm1Defr/J Stock No: 008888), Rag2 KO (B6(Cg)-Rag2tm1.1Cgn/J Stock No: 008449). *Apc*$^{loxp\ exon\ 14}$ (Apc$^{L/L}$) has been previously described(Colnot et al., 2004). *Villin-CreERT2* was a gift from Sylvie Robine. Diet-induced obesity studies were performed by using a high fat diet consisting of 60 kcal% fat (Research Diets D12492) beginning at the age of 8-12 weeks and extending for 9 to 14 months. Control mice were age- and sex-matched and were fed matched purified control diet (Research Diets, D12450J). GW501516 (Enzo) was reconstituted in DMSO at 4.5 mg ml^{-1} and diluted 1:10 in a solution of 5% PEG400 (Hampton Research), 5% Tween80 (Sigma), 90% H_2O (injection buffer) for a daily intraperitoneal injection of 4mg kg^{-1}. Alleles crossed with Lgr5-CreERT2 (to generate stem cell specific knockout, Lgr5-iKO) or Villin-CreERT2 (to generate intestinal epithelium specific knockout, vil-iKO) mice were excised by administration of tamoxifen suspended in sunflower seed oil (Spectrum S1929) at a concentration of 10 mg ml^{-1} and 250 μL per 25 g of body weight, and administered by intraperitoneal injection every other day for 4 times. BrdU (Sigma) was prepared at 10 mg ml^{-1} in PBS, passed through 0.22 μm filter and injected at 100mg kg^{-1}. CYT387 (SelleckChem) was reconstituted in DMSO at 10mg ml^{-1} and diluted 1:100 in injection buffer for a daily gavage of 25mg kg^{-1} for 7 days. CL429 (InvivoGen) was reconstituted in DMSO at 5mg ml^{-1} and diluted 1:20 in a solution of injection buffer for a daily gavage of 2mg kg^{-1} for 7 days. For broad-spectrum antibiotic treatment, mice received a mixture of vancomycin (0.5g/l), ampicillin (1g/l), metronidazole (1g/l) and neomycin (1g/l) in the drinking water. Sex- and age-matched animals between 8 and 12 weeks of age were used for experiments unless otherwise specified. To estimate proper number of animals, preliminary experiments were performed. Mice were allocated at random to experimental groups. The Institutional Animal Care and Use Committee (IACUC) at CSHL, Boston Children's Hospital and Massachusetts Institute of Technology approved all animal experiments.

METHOD DETAILS

Immunohistochemistry (IHC)

As previously described(Yilmaz et al., 2012), tissues were fixed in 10% formalin, paraffin embedded and sectioned. Antigen retrieval was performed with Borg Decloaker RTU solution (Biocare Medical) in a pressurized Decloaking Chamber (Biocare Medical) for 3 minutes. Antibodies used: rat anti-BrdU (1:2000, Abcam 6326), mouse monoclonal β-catenin (1:100, BD Biosciences 610154), rabbit monoclonal OLFM4 (1:10,000, gift from CST, clone PP7), rat anti-CD3 (1:200, eBioscience, clone 145-2C11), rat anti-CD4, (1:200, Biolegend, clone H129.19), rat anti-CD8 (1:200, Biolegend, clone 53-6.7), anti-Ki67 (1:200, Thermo Fisher, MA5-14520). Biotin-conjugated secondary donkey anti-rabbit or anti-rat antibodies were used from Jackson ImmunoResearch. The Vectastain Elite ABC immunoperoxidase detection kit (Vector Labs) followed by Dako Liquid DAB+ Substrate (Dako) was used for visualization. All antibody incubations involving tissue or sorted cells were performed with Common Antibody Diluent (Cell Signaling).

In situ hybridization

Single-molecule *in situ* hybridization was performed to detect MHC-II (H2-Ab1, #414731) using Advanced Cell Diagnostics RNAscope 2.5 HD Detection Kit following manufacturer's instructions.

Intestinal crypt isolation and flow cytometry

As previously reported(Beyaz et al., 2016) and briefly summarized here, small intestines and colons were removed, washed with cold PBS−/−, opened laterally and cut into 3-5mm fragments. Pieces were washed multiple times with cold PBS−/− until clean, washed 2-3 with PBS−/−/EDTA (10mM), and incubated on ice for 90-120 minutes while mixing at 30-minute intervals. Crypts were then mechanically separated from the connective tissue by shaking, and filtered through a 70-μm mesh into a 50 mL conical tube to remove villus material (for small intestine) and tissue fragments. Crypts were removed from this step for crypt culture experiments and embedded in Matrigel^{TM} with crypt culture media. For ISC isolation, the crypt suspensions were dissociated to individual cells with TrypLE Express (Invitrogen) and stained for flow cytometry. ISCs were isolated as Lgr5-EGFP^{hi}Epcam^{+} CD45^{-}7-AAD^{-} with a BD FACS Aria II SORP cell sorter into supplemented crypt culture medium for culture.

Organoid culture for crypts and isolated cells

Isolated crypts were counted and embedded in Matrigel^{TM} (Corning 356231 growth factor reduced) at 5–10 crypts per μl and cultured in a modified form of medium as described previously(Sato et al., 2009). Unless otherwise noted, Advanced DMEM (GIBCO) was supplemented by EGF 40 ng ml^{-1} (R&D), Noggin 200 ng ml^{-1} (Peprotech), R-spondin 500 ng ml^{-1} (R&D or Sino Biological),

Please cite this article in press as: Beyaz et al., Dietary suppression of MHC class II expression in intestinal epithelial cells enhances intestinal tumorigenesis, Cell Stem Cell (2021), https://doi.org/10.1016/j.stem.2021.08.007

N-acetyl-L-cysteine 1 μM (Sigma-Aldrich), N2 1X (Life Technologies), B27 1X (Life Technologies), Chiron 10 μM (Stemgent), Y-27632 dihydrochloride monohydrate 20 ng ml^{-1} (Sigma-Aldrich). 25 μL drops of Matrigel™ with crypts were plated onto a flat bottom 48-well plate (Corning 3548) and allowed to solidify for 20 minutes in a 37°C incubator. Three hundred microliters of crypt culture medium were then overlaid onto the Matrigel™, changed every three days, and maintained at 37°C in fully humidified chambers containing 5% CO_2. Clonogenicity (colony-forming efficiency) was calculated by plating 50–300 crypts per well and assessing organoid formation 3–7 days or as specified after initiation of cultures. Organoids were propagated for perturbation experiments as previously described(Beyaz et al., 2016).

Isolated ISCs or progenitor cells were centrifuged for 5 minutes at 250 g, re-suspended in the appropriate volume of crypt culture medium (500–1,000 cells μl^{-1}), then seeded onto 25-30 μL Matrigel™ (Corning 356231 growth factor reduced) containing 1 μM Jagged (Ana-Spec) in a flat bottom 48-well plate (Corning 3548). Alternatively, ISCs and Paneth cells were mixed after sorting in a 1:1 ratio, centrifuged, and then seeded onto Matrigel™. The Matrigel™ and cells were allowed to solidify before adding 300 μL of crypt culture medium. The crypt media was changed every second or third day. Organoid bodies were quantified on days 3, 7 and 10 of culture, unless otherwise specified. In secondary experiments, individual primary organoids were mechanically dissociated and replated, or organoids were dissociated for 10 minutes in TrypLE Express at 32°C, resuspended with SMEM (Life Technologies), centrifuged and resuspended in cold SMEM with viability dye 7-AAD. Live cells were sorted and seeded onto Matrigel™ as previously described(Beyaz et al., 2016).

DQ-Ovalbumin Assay

Sorted Lgr5+ intestinal stem cells were plated in Matrigel and crypt media for one day. The following day, the crypt media was replaced with crypt media containing 20 μg/mL DQ-ovalbumin (Thermo Fisher, D12053) and cells were incubated at 4C and 37C for 24 hours. Cells were harvested by washing three times in PBS, removing the Matrigel using Cell Recovery Solution (Corning) and filtered through a 40 μm mesh. Mean fluorescent intensity was analyzed using CellSimple (Cell Signaling).

Bulk RNA-Seq Analysis

Processing of RNA-seq reads and measuring expression level. Tha raw data processed using RNA-Seq pipeline in DolphinNext with following steps(Yukselen et al., 2020). Raw stranded reads (40 nt) were trimmed to remove adaptor and bases with quality scores below 20, and reads shorter than 35 nt were excluded. High-quality reads were mapped to the mouse genome (mm10) with TopHat version 1.4.1 (Trapnell et al., 2009), using known splice junctions from Ensembl Release 70 and allowing at most 2 mismatches. Genes were quantified with htseq-count (with the ''intersect strict'' mode) using Ensembl Release 70 gene models. Gene counts were normalized across all samples using estimateSizeFactors() from the DESeq R/Bioconductor package(Anders and Huber, 2010). Differential expression analysis made with DESeq2 package using DEBrowser(Kucukural et al., 2019).

qRT-PCR

Cells were sorted into Tri Reagent (Life Technologies) and total RNA was isolated according to the manufacturer's instructions with following modification: the aqueous phase containing total RNA was purified using RNeasy plus kit (QIAGEN). RNA was converted to cDNA with cDNA synthesis kit (Bio-Rad). qRT-PCR was performed with SYBR green master mix (Bio-Rad) on Bio-Rad iCycler RT-PCR detection system. For low cell numbers (< 1000), qRT-PCR was performed after sequence specific pre-amplification as described previously(Beyaz et al., 2017). Primers are listed in Table S3.

Single cell RNA-Seq

Cell sorting

FACS (Astrios) was used to sort one single cell into each well of a 96-well PCR plate containing 5μl of TCL buffer with 1% 2-mercaptoethanol. The cells were stained for $7AAD^-$ (Life Technologies), $CD45^-$ (eBioscience), $CD31^-$ (eBioscience), $Ter119^-$ (eBioscience), $EpCAM^+$ (eBioscience). To enrich for specific IEC populations, cells were isolated from control or HFD Lgr5-GFP mice, stained with the antibodies mentioned above and gated for GFP-high (stem cells). A population control of 200 cells was sorted into one well and a no-cell control was sorted into another well. After sorting, the plate was sealed tightly with a Microseal F and centrifuged at 800 g for 1 min. The plate was immediately frozen on dry ice and kept at −80°C until ready for the lysate cleanup.

Plate-based scRNA-seq

Libraries were prepared using a modified SMART-Seq2 protocol as previously reported (Picelli et al., 2014). Briefly, RNA lysate cleanup was performed using RNAClean XP beads (Agencourt), followed by reverse transcription with Maxima Reverse Transcriptase (Life Technologies) and whole transcription amplification (WTA) with KAPA HotStart HIFI 2 × ReadyMix (Kapa Biosystems) for 21 cycles. WTA products were purified with Ampure XP beads (Beckman Coulter), quantified with Qubit dsDNA HS Assay Kit (ThermoFisher), and assessed with a high sensitivity DNA chip (Agilent). RNA-seq libraries were constructed from purified WTA products using Nextera XT DNA Library Preparation Kit (Illumina). On each plate, the population and no-cell controls were processed using the same method as the single cells. The libraries were sequenced on an Illumina NextSeq 500.

Computational analysis of scRNA-seq

We profiled Lgr5-high ISCs sorted from control (n = 192 cells) and HFD (n = 192 cells) using a full length scRNA-seq method (Picelli et al., 2014). Each condition included two replicate 96-well plates from 2 different mice. Expression levels of gene loci were quantified using RNA-seq by Expectation Maximization (RSEM) (Li and Dewey, 2011). Raw reads were mapped to a mouse transcriptome index

(mm10 UCSC build) using Bowtie 2 (Langmead and Salzberg, 2012), as required by RSEM in its default mode. On average, 90% of the reads mapped to the genome in every sample. and 55% of the reads mapped to the transcriptome. RSEM yielded an expression matrix (genes x samples) of inferred gene counts, which was converted to TPM (transcripts per million) values and then log-transformed after the addition of 1 to avoid zeros. After filtering cells with low QC metrics (< 400,000 mapped reads, transcriptomic mapping rate < 35% and < 1500 genes detected), we selected 171 control cells and 144 HFD cells for further analysis. We identified 379 highly variable genes using Seurat's MeanVarPlot function. H2-Ab1, a key component of MHC-II complex, was among the top 5 differentially expressed genes with > 3-fold higher expression in control compared to HFD ISCs as assessed using Model-based Analysis of Single-cell Transcriptomics (MAST) test.(Finak et al., 2015) A Gene Ontology analysis of these genes against a background of genes matched in average expression levels showed an enrichment of terms consistent with intestinal biology such as arachidonic acid metabolic process (GO:0019369), intestinal absorption (GO:0050892), as well as immune response, such as "antigen processing and presentation of exogenous peptide antigen" (GO:0002478) and "defense response to Gram-negative (GO:0050829), and Gram-positive (GO:0050830) bacterium." We performed principal component analysis (PCA) on the data based on the variable genes, and embedded 10 statistically significant PCs identified using a permutation test (Shekhar et al., 2016) on a 2D map using t-distributed stochastic neighbor embedding (tSNE).

Taxonomic microbiota analysis

Frozen fecal samples were processed for DNA isolation using the QIAGEN PowerSoil kit according to the manufacturer's instructions. 1 ng of purified fecal DNA was used for PCR amplification. Amplicons spanning the variable region 1/2 (V1/2) of the 16S rRNA gene were generated by using the following barcoded primers: Fwd 5′-XXXXXXXXAGAGTTTGATCCTGGCTCAG-3′, Rev 5′-TGCTGCCTCCCGTAGGAGT-3′, where X represents a barcode base. The reactions were subsequently pooled and cleaned, and the PCR products were then sequenced on an Illumina MiSeq with 500 bp paired-end reads. The reads were then processed using the QIIME (Quantitative Insights Into Microbial Ecology, http://www.qiime.org) analysis pipeline. Rarefaction was used to exclude samples with insufficient count of reads per sample. Sequences sharing 97% nucleotide sequence identity in the 16S region were binned into operational taxonomic units (97% ID OTUs). For beta-diversity, unweighted UniFrac measurements were plotted according to the two principal coordinates based on > 10,000 reads per sample.

Endoscopy-guided orthotopic tumor transplantation and injections

Lgr5-EGFP-IRES-CreERT2; Apc$^{L/L}$ mice were injected with two doses of tamoxifen I.P. Four days later, *Apc* null Lgr5-GFP^{hi} ISCs and Lgr5-GFP^{low} progenitors were sorted by flow cytometry, as described above. For primary cell transplantations, 10,000 *Apc* null Lgr5-GFP^{hi}, MHC^{hi} and MHC^{low} ISCs were resuspended into 90% crypt culture media (as described) and 10% Matrigel^{TM}, and then transplanted into the colonic lamina propria of C57BL/6 recipient mice as previously described (Beyaz et al., 2016; Roper et al., 2017). Mice then underwent colonoscopy eight weeks later to assess tumor formation. Colonoscopy videos and images were saved for offline analysis. Following sacrifice, the distal colons were excised and fixed in 10% formalin, then examined by histology to identify adenomas. In addition, colon tumors were induced in *VillinCreERT2; Apc*$^{L/L}$ mice and VillinCreERT2; *Apc*$^{L/L;\ MHC\text{-}IIL/L}$ mice, as previously described (Roper et al., 2017, 2018). Tumors were monitored with optical colonoscopy for two weeks. Offline images were analyzed using ImageJ to calculate Tumor Size Index, as previously described(Roper et al., 2011). Finally, Lgr5CreERT2; MHC-II$^{L/+}$; APC$^{L/+}$ and Lgr5CreERT2; MHC-II$^{L/+}$; APC$^{L/+}$ mice were treated with tamoxifen suspended in sunflower seed oil (Spectrum S1929) at a concentration of 10 mg ml^{-1} and 250 μL per 25 g of body weight by intraperitoneal injection every other day for 4 times and followed for 5 months to assess tumor formation by histology. All tumor histology images were reviewed by gastrointestinal pathologists who were blinded to treatment groups.

QUANTIFICATION AND STATISTICAL ANALYSIS

Unless otherwise specified, all experiments reported in this study were repeated at least five independent times and sample number (n) represents biological replicates. For murine organoid assays, 2-5 wells per mouse per *ex vivo* treatment were analyzed. All center values shown in graphs refer to the mean. No sample or animals were excluded from analysis and sample size estimates were not used. Animals were randomly assigned to groups. Experiments used roughly equivalent male and female mice to account for sex as a biological variable. Studies were not conducted blind with the exception of all histological analyses.